Super-Grid Modeling of the Elastic Wave Equation in Semi-Bounded Domains

N. Anders Petersson[*] and Björn Sjögreen

Center for Applied Scientific Computing, L-422, LLNL, P.O. Box 808, Livermore, CA 94551, USA.

Abstract. We develop a super-grid modeling technique for solving the elastic wave equation in semi-bounded two- and three-dimensional spatial domains. In this method, waves are slowed down and dissipated in sponge layers near the far-field boundaries. Mathematically, this is equivalent to a coordinate mapping that transforms a very large physical domain to a significantly smaller computational domain, where the elastic wave equation is solved numerically on a regular grid. To damp out waves that become poorly resolved because of the coordinate mapping, a high order artificial dissipation operator is added in layers near the boundaries of the computational domain. We prove by energy estimates that the super-grid modeling leads to a stable numerical method with decreasing energy, which is valid for heterogeneous material properties and a free surface boundary condition on one side of the domain. Our spatial discretization is based on a fourth order accurate finite difference method, which satisfies the principle of summation by parts. We show that the discrete energy estimate holds also when a centered finite difference stencil is combined with homogeneous Dirichlet conditions at several ghost points outside of the far-field boundaries. Therefore, the coefficients in the finite difference stencils need only be boundary modified near the free surface. This allows for improved computational efficiency and significant simplifications of the implementation of the proposed method in multi-dimensional domains. Numerical experiments in three space dimensions show that the modeling error from truncating the domain can be made very small by choosing a sufficiently wide super-grid damping layer. The numerical accuracy is first evaluated against analytical solutions of Lamb's problem, where fourth order accuracy is observed with a sixth order artificial dissipation. We then use successive grid refinements to study the numerical accuracy in the more complicated motion due to a point moment tensor source in a regularized layered material.

AMS subject classifications: 65M06, 74S20, 86A15

Key words: Far field boundary conditions, higher order methods, elastic wave equation, summation by parts.

---

[*]Corresponding author. *Email addresses:* `petersson1@llnl.gov` (N. A. Petersson), `sjogreen2@llnl.gov` (B. Sjogreen)

1 Introduction

To numerically solve a time-dependent wave equation in an unbounded spatial domain, it is necessary to truncate the domain and impose a far-field closure at, or near, the boundaries of the truncated domain. Numerous different approaches have been suggested, see for example [4, 6, 16]. The perfectly matched layer (PML) technique, originally proposed by Berenger [3] and later improved by many others, has been very successful for electromagnetic wave simulations. Unfortunately, the PML technique sometimes suffers from stability problems when applied to the elastic wave equation, where free surface boundaries and material discontinuities can form wave guides in which the solution of the PML system becomes unstable [18]. The PML system is also known to exhibit stability problems for some anisotropic wave equations [2].

Similar to the PML technique, the super-grid method [1] modifies the original wave equation in layers near the boundary of the computational domain. The PML system is defined by Fourier transforming the original wave equation in time and applying a frequency-dependent complex-valued coordinate transformation in the layers. Additional dependent variables, governed by additional differential equations, must be introduced to define the PML system in the time domain. In comparison, the super-grid method is based on applying a real-valued coordinate stretching in the layers, where also artificial dissipation is added. The super-grid method does not rely on additional dependent variables, and is therefore more straight forward to implement. In the layers near the boundary, the PML method damps the waves; in contrast, the super-grid method both damps the waves and slows them down. The main advantage over the PML technique is that the solution of the wave equation with super-grid layers is energy stable, if there is a corresponding energy estimate for the underlying wave equation.

In this article, we generalize the super-grid approach [1] to the elastic wave equation in second order formulation. Motivated by applications from seismology and seismic exploration, we focus on half-plane or half-space domains, where a free surface boundary condition must be satisfied on only one side of the domain. The half-space problem subject to a free surface condition permits surface waves. These waves only propagate along the free surface and decay exponentially away from the surface. They are fundamentally different from the longitudinal and transverse waves that travel through the volume of the domain. Surface waves therefore constitute an additional type of wave that need to be absorbed by the far-field closure.

We are primarily interested in cases where the solution is of a transient nature, being driven by initial data with compact support, or by a forcing function that only is active (non-zero) for a limited time. Because of the artificial damping in the super-grid layers, the solution becomes very small on the outside of the layers. For this reason, it is natural to impose homogeneous Dirichlet conditions at the super-grid boundaries, which truncate the computational domain. In this paper, we develop a finite difference method where fourth order accurate summation by parts (SBP) operators [17] are combined with centered fourth order accurate finite difference formulas in the interior of the

domain. The idea is to only use the SBP operators near the free surface boundary, and use centered finite difference formulas all the way up to the super-grid boundaries. This is made possible by enforcing homogeneous Dirichlet boundary conditions at several grid points outside the super-grid boundaries. This simplified boundary closure allows the implementation of the super-grid approach to be more efficient and greatly simplified in multi-dimensional domains, because the SBP operators are only needed near the free surface boundary.

SBP operators make it possible to prove stability for a difference approximation by mimicking the integration by parts estimate for the partial differential equation. In the interior of the domain, these operators are centered finite difference formulas. To satisfy the principle of SBP, the difference formulas must become biased and have coefficients that are different for each grid point near a boundary. We call the discretization technique in [17] SBP-GP because it uses ghost points. These points are located just outside the boundary, and are used to enforce the boundary conditions strongly. There is also a related approach, called SBP-SAT [9,10], which uses penalty terms to enforce the boundary conditions weakly. In principle, either of these SBP discretizations could be used to solve the elastic wave equation with super-grid layers.

The main theoretical result of this article is that stability of the numerical method can be proven also when the SBP operators are combined with centered operators, together with our simplified boundary closure near the super-grid boundaries. This leads to an overall spatial discretization that does not satisfy the principle of SBP, but nevertheless is energy stable. Note that the simplified boundary closure is intimately related to the super-grid method. It can only lead to an accurate approximation if the solution is very small near the super-grid boundary and is not appropriate for cases with inhomogeneous boundary data.

This paper continues the development of the super-grid method, with an emphasis on wave equations in second order formulation and multi-dimensional domains. While most of the development in [1] was done for hyperbolic systems in first order formulation in the continuous (PDE) setting, we focus on the elastic wave equation and establish stability results for the fully discrete approximation. We also present a new damping function for the super-grid layers, which gives the strongest damping in the outer parts of the supergrid layers. As a result, the suppression of outgoing waves is improved compared to the damping function used in [1]. A new tapering approach is introduced to scale the damping functions near edges and corners in multi-dimensional domains, such that the strength of the damping along the sides of the domain does not have to be reduced to meet the stability constraints of the explicit time integrator.

The remainder of the paper is organized in the following way. The super-grid method is first outlined in Section 1.1. In Section 2, we generalize our fourth order accurate time integration scheme [17] to the 1-D wave equation with grid stretching and artificial dissipation in the super-grid layers. We present our simplified boundary closure for the discretization that enables the centered difference stencils to be used all the way up to the super-grid boundaries. Because we solve the wave equation in second order for-

mulation, the artificial dissipation contains a time derivative. We present an explicit time discretization and apply the energy method to prove stability of the fully discrete scheme. We outline a von Neumann analysis to show how the coefficient of the artificial dissipation must scale with the grid size to avoid a reduction of the explicit time step. It also exposes the stability limit of the amplitude of the damping function.

In Section 3 we generalize the results to the half-plane problem for the two-dimensional elastic wave equation subject to a free surface boundary condition along the physical boundary. The spatial discretization combines the SBP boundary modified stencils at the free surface boundary with our simplified boundary closure at the super-grid boundaries. The super-grid damping is introduced dimension by dimension and the energy method is used to show that the fully discrete scheme is stable. Our energy estimate shows that the strengths of the one-dimensional damping terms are accumulated near corners, where two super-grid layers meet. A two-dimensional von Neumann analysis illustrates that the explicit time step is limited by the sum of the strengths of the one-dimensional dissipation terms. To avoid having to either reduce the amplitude of the damping functions away from corners, or impose additional time step restrictions, we present a tapering approach that reduces the strength of the one-dimensional damping functions near corners.

The reflection properties of the super-grid method are evaluated numerically by solving the three-dimensional elastic wave equation in Section 4. We first consider Lamb's problem, where the numerical solution is compared to an analytical solution. We also test the accuracy on a regularized layered material model, where the convergence is assessed by successive grid refinements. Conclusions are given in Section 5.

1.1 Outline of the supergrid method

Consider solving a time-dependent wave equation in an unbounded or semi-bounded (half-space) domain. Assume that we wish to calculate the numerical solution in a finite time interval $0 \leq t \leq t_{\max}$, in the bounded spatial domain $\mathbf{x} \in \bar{\Omega} \in \mathbb{R}^d$ ($d = 1,2,3$). We will call this the domain of interest. For $d = 3$ this could, for example, be a box shaped domain $\bar{\Omega} = \{x_1 \leq x \leq x_2, \, y_1 \leq y \leq y_2, \, z_1 \leq z \leq z_2\}$, where $\mathbf{x} = (x,y,z)^T$ are the Cartesian coordinates. Also assume that the initial conditions and forcing functions have compact support in $\bar{\Omega}$. While the numerical solution may be calculated in a computational domain that is larger than $\bar{\Omega}$, it must eventually be truncated to a finite extent. In general, the truncation of the computational domain leads to artificial reflections that can pollute the numerical solution in the domain of interest. However, due to the hyperbolic nature of wave equations, no artificial reflections can enter $\bar{\Omega}$ for $t \leq t_{\max}$, if the computational domain is sufficiently large. For example, if the computational domain is given by $x_1 - L \leq x \leq x_2 + L$, reflections from the outer boundary can only pollute the solution in the subdomain $x_1 \leq x \leq x_2$ for times $t > t_L = 2L/c_{\max}$. Here, $c_{\max}$ is the largest phase velocity in the domain. Hence, by choosing $L \geq t_{\max} c_{\max}/2$, we can avoid all artifacts from the truncation of the computational domain, up to time $t = t_{\max}$. Unfortunately, the size of the computational domain

would grow with t_{max} and could easily become much larger than the original domain of interest. Hence, this simple approach is computationally intractable unless the grid size can be made significantly larger outside the domain of interest, without polluting the numerical solution with poorly resolved modes.

The first ingredient of the super-grid approach [1] is to introduce a smooth coordinate transformation,

$$x = X(\xi), \quad y = Y(\eta), \quad z = Z(\zeta),$$

that maps the computational domain onto a much larger extended domain. For example, in the x-direction, $x_1 - \ell \leq \xi \leq x_2 + \ell$ is mapped onto $x_1 - L \leq x \leq x_2 + L$, where $\ell \ll L$. The original wave equation is solved inside the domain of interest, i.e., the identity mapping $x = \xi$ is used for $x_1 \leq \xi \leq x_2$. The parts of the computational domain that are *outside* of the domain of interest are called the super-grid layers, i.e., $x_1 - \ell \leq \xi < x_1$ and $x_2 < \xi \leq x_2 + \ell$.

Spatial derivatives in the wave equation are transformed according to the chain rule,

$$\frac{\partial}{\partial x} = \phi^{(x)}(\xi)\frac{\partial}{\partial \xi}, \quad \frac{\partial}{\partial y} = \phi^{(y)}(\eta)\frac{\partial}{\partial \eta}, \quad \frac{\partial}{\partial z} = \phi^{(z)}(\zeta)\frac{\partial}{\partial \zeta}, \tag{1.1}$$

where

$$\phi^{(x)}(\xi) = \frac{1}{X'(\xi)}, \quad \phi^{(y)}(\eta) = \frac{1}{Y'(\eta)}, \quad \phi^{(z)}(\zeta) = \frac{1}{Z'(\zeta)}.$$

To make the coordinate transformation non-singular, we assume $\phi^{(q)} \geq \varepsilon_L > 0$, $q = x, y, z$.

For a one-dimensional Cauchy problem, $\phi^{(x)}$ needs to be a smooth function that transitions monotonically from ε_L to 1 between $x_1 - \ell$ and x_1, and then back to ε_L between x_2 and $x_2 + \ell$, see Fig. 1. For higher dimensional problems, the functions $\phi^{(y)}$ and $\phi^{(z)}$ are defined in a corresponding way.

In the mapped (computational) coordinates, the length scale of the solution in the ξ-direction is proportional to $\phi^{(x)}$. The solution is therefore compressed inside the layers, where $\phi^{(x)} < 1$. This corresponds to a slowing down of all traveling waves in the mapped coordinates. Note that in a two-dimensional domain, $\phi^{(x)} < 1$ corresponds to a slow down in the ξ-direction, while $\phi^{(y)} < 1$ gives a slow down in the η-direction. Hence, if the original wave equation has isotropic wave propagation properties, it becomes anisotropic in the mapped coordinates. The case of a half-plane problem in two space dimensions is illustrated in Fig. 2.

The super-grid method discretizes the mapped (computational) domain on a grid with constant spacing. For this reason, the resolution in terms of grid points per wave length will be very poor in the layers. To avoid polluting the numerical solution by modes that can not be resolved on the grid, the second essential ingredient of the super-grid method is the addition of artificial damping. The dissipative term is only added in the layers and, for efficiency reasons, only explicit discretizations are considered. The idea is to damp out poorly resolved waves before they arrive at the outer edge of the layer, where the computational domain is truncated. As was emphasized in [1], it is important
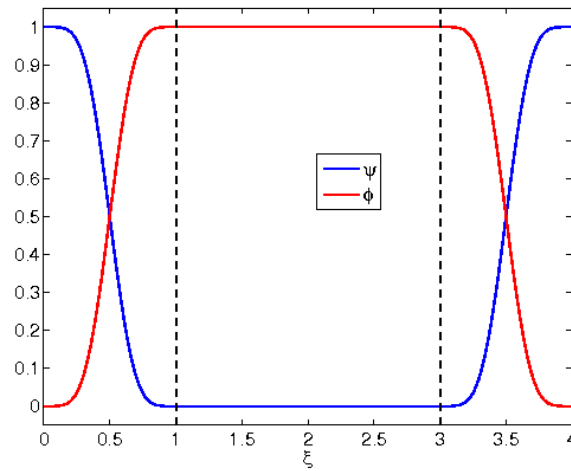
Figure 1: The stretching function $\phi(\xi)$ (red) and the auxiliary function $\psi(\xi)$ (blue), which controls the strength of the damping. In this case, the width of each super-grid layer is $\ell=1$. The dashed vertical lines indicate the boundaries of the domain of interest, here $1 \leq \xi \leq 3$.

Figure 2: A two-dimensional half-plane domain with a physical boundary along the top edge. The stretching functions satisfy $\phi^{(x)}=\phi^{(y)}=1$ in the white region, where the original wave equation is solved. The wave speed is reduced in the surrounding layers by taking $\phi^{(x)}<1$ (red) and $\phi^{(y)}<1$ (blue). In the purple corner regions, $\phi^{(x)}<1$ and $\phi^{(y)}<1$.

to use a damping term of sufficiently high order, such that it does not dominate the truncation error in the interior of the domain. The strength of the dissipation is controlled by the auxiliary function ψ (see Fig. 1), which must be ramped up smoothly to avoid artificial reflections. The amplitude of the damping must be large enough to damp out the solution before it is reflected back into the domain of interest. However, that amplitude is also restricted by the stability limit of the explicit time stepping scheme. Numerical experiments show that the super-grid method gives the best performance when the amplitude of the damping is close to the stability limit.

2   The scalar wave equation in one space dimension

Consider the Cauchy problem for the one-dimensional scalar wave equation,

$$\rho \frac{\partial^2 u}{\partial t^2} = \frac{\partial}{\partial x}\left(\mu \frac{\partial u}{\partial x}\right) + f(x,t), \quad -\infty < x < \infty, \quad t \geq 0,$$

$$u(x,0) = g_0(x), \quad u_t(x,0) = g_1(x), \quad -\infty < x < \infty. \tag{2.1}$$

Here $\rho = \rho(x) > 0$ and $\mu = \mu(x) > 0$ are material coefficients that may vary in space, $g_0(x)$ and $g_1(x)$ are the initial data, and $f(x,t)$ is the external forcing function. The forcing and initial data are assumed to have compact support in the sub-domain $x \in \bar{\Omega}$ where $\bar{\Omega} = \{x_1 \leq x \leq x_2\}$. This is also assumed to be the domain of interest, i.e., where we want to find a numerical solution of (2.1).

We add a super-grid layer of width $\ell > 0$ on either side of $\bar{\Omega}$, and choose the coordinate system such that $x_1 - \ell = 0$ and $x_2 + \ell = x_{\max}$. After introducing the coordinate mapping (1.1) (using the simplified notation $\phi = \phi^{(x)}$) and introducing a super-grid dissipation of order $2p$, we obtain the modified wave equation

$$\rho \frac{\partial^2 v}{\partial t^2} = \phi \frac{\partial}{\partial \xi}\left(\phi \mu \frac{\partial v}{\partial \xi}\right) - \varepsilon(-1)^p \phi \frac{\partial^p}{\partial \xi^p}\left(\sigma \rho \frac{\partial^p v_t}{\partial \xi^p}\right) + f(X(\xi),t), \tag{2.2}$$

for $0 \leq \xi \leq x_{\max}$ and $t \geq 0$, where $\varepsilon > 0$. The solution of (2.2) is subject to the initial conditions

$$v(\xi,0) = g_0(X(\xi)), \quad v_t(\xi,0) = g_1(X(\xi)), \quad 0 \leq \xi \leq x_{\max}. \tag{2.3}$$

The stretching function $\phi(x)$ and the damping function $\sigma(x)$ are constructed from the auxiliary function $\psi(x)$, which smoothly transitions from one to zero and then back to one,

$$\psi(x) = \begin{cases} 1, & x \leq x_1 - \ell, \\ P((x_1 - x)/\ell), & x_1 - \ell < x < x_1, \\ 0, & x_1 \leq x \leq x_2, \\ P((x - x_2)/\ell), & x_2 < x < x_2 + \ell, \\ 1, & x \geq x_2 + \ell. \end{cases} \tag{2.4}$$

Here we use the polynomial function $P(\xi) = \xi^6(462 - 1980\xi + 3465\xi^2 - 3080\xi^3 + 1386\xi^4 - 252\xi^5)$, which satisfies $P(0) = 0$, $P(1) = 1$, and makes $\psi(\xi)$ five times continuously differentiable. The one-dimensional stretching and damping functions are defined by

$$\phi(x) = 1 - (1 - \varepsilon_L)\psi(x), \qquad \sigma(x) = \frac{\psi(x)}{\phi(x)}. \tag{2.5}$$

Note that the constant $\varepsilon_L > 0$ is not related to the damping coefficient ε in (2.2). Throughout the numerical experiments in this paper, we use $\varepsilon_L = 10^{-4}$. The functions ψ and ϕ are plotted in Fig. 1.

The stretching and damping functions only modify the original wave equation inside the supergrid layers, because $\phi(x)=1$ and $\sigma(x)=0$, for $x_1 \leq x \leq x_2$. Also note the factor $\rho\sigma$ in the dissipation term in (2.2). Here, ρ is included to make this term balance the left hand side of the equation, i.e., to make ε independent of ρ.

We proceed by deriving an energy estimate. Note that the regular L_2 scalar product can be used to derive an energy estimate for the original wave equation (2.1). To estimate the solution of (2.2) it is therefore natural to weigh the scalar product by the stretching function (1.1). For real-valued functions $v(\xi)$ and $w(\xi)$, we define

$$(v,w)_\phi = \int_0^{x_{\max}} \frac{v(\xi)w(\xi)}{\phi}d\xi, \qquad \|v\|_\phi^2 = (v,v)_\phi,$$

where $\|v\|_\phi$ is a norm because $\phi \geq \varepsilon_L > 0$.

Assume that $f=0$ and multiply the differential equation (2.2) by v_t/ϕ and integrate over $0 \leq x \leq x_{\max}$. After integration by parts, we get

$$(v_t,\rho v_{tt})_\phi + (v_{t\xi},\phi^2\mu v_\xi)_\phi = -\varepsilon\left(\frac{\partial^p v_t}{\partial\xi^p},\phi\sigma\rho\frac{\partial^p v_t}{\partial\xi^p}\right)_\phi + BT,$$

where the boundary term satisfies

$$BT = \left[v_t\phi\mu v_\xi\right]_0^{x_{\max}} - \varepsilon(-1)^p\left[\left(v_t\frac{\partial^{p-1}}{\partial\xi^{p-1}}-\cdots+(-1)^{p-1}\frac{\partial^{p-1}v_t}{\partial\xi^{p-1}}\right)\left(\sigma\rho\frac{\partial^p v_t}{\partial\xi^p}\right)\right]_0^{x_{\max}}. \quad (2.6)$$

The boundary term vanishes if we impose the following p boundary conditions at $\xi=0$ and $\xi=x_{\max}$,

$$v(0,t)=0, \qquad\qquad v(x_{\max},t)=0,$$
$$v_\xi(0,t)=0, \qquad\qquad v_\xi(x_{\max},t)=0,$$
$$\vdots \qquad\qquad\qquad \vdots$$
$$\frac{\partial^{p-1}v}{\partial\xi^{p-1}}(0,t)=0, \qquad \frac{\partial^{p-1}v}{\partial\xi^{p-1}}(x_{\max},t)=0, \qquad t\geq 0. \quad (2.7)$$

We define the energy by $E(t)=\frac{1}{2}(v_t,\rho v_t)_\phi+\frac{1}{2}(\phi v_\xi,\phi\mu v_\xi)_\phi$, which is a norm because $\rho>0$, $\mu>0$, and $\phi\geq\varepsilon_L>0$. We arrive at

$$\frac{d}{dt}E(t) = -\varepsilon\left(\frac{\partial^p v_t}{\partial\xi^p},\phi\sigma\rho\frac{\partial^p v_t}{\partial\xi^p}\right)_\phi \leq 0. \quad (2.8)$$

Hence, $E(t) \leq E(0)$ for $t>0$. Assuming that the solution of the initial boundary value problem (2.2), (2.3), (2.7) exists[†], we conclude that is well-posed if $\varepsilon\geq 0$.

[†]Existence of solutions of the corresponding first order system with super-grid dissipation follows from Theorem 7.8.1 in [7]. Additional analysis would be required to establish existence of solutions of the wave equation considered here, but this is beyond the scope of the present article.

Because $E(t)$ is scaled by ρ, the strength of the damping in the super-grid layers is determined by the product $\varepsilon\phi\sigma$. This motivates our construction of $\sigma(x)$ in (2.5), which satisfies $\phi(x)\sigma(x)=\psi(x)\to 1$ for $x\to 0$ and $x\to x_{\max}$. Our construction makes the damping the strongest in the outer parts of the super-grid layers. We remark that our construction is different from that used in [1], where the damping function satisfies $\sigma(x)\to 1$ for $x\to 0$ and $x\to x_{\max}$. Because the strength of the damping is determined by the product $\sigma\phi$, the construction used in [1] gives a damping that is the strongest near the middle of the super-grid layers, and very weak in the outer parts of the super-grid layers, because $\phi\sigma\to\varepsilon_L\ll 1$ for $x\to 0$ and $x\to x_{\max}$.

2.1 Discretizing the wave equation with super-grid layers

The theoretical properties of the discretization developed in this and the following sections builds to a large extent on the basic theory developed in [17]. Familiarity with that paper will expedite the understanding of the theory developed here.

We discretize the one-dimensional spatial domain on the uniform grid $\xi_j=(j-1)h$, $j=1-\tilde{p},\cdots,1,2,3,\cdots,N_x+\tilde{p}$, where $\tilde{p}$ is the number of ghost points (to be defined below). The constant grid spacing, $h>0$, is chosen such that $\xi_{N_x}=x_{\max}$. Time is discretized by $t_n=n\Delta_t$, where $n=0,1,2,\cdots$ and $\Delta_t>0$ is the constant time step. The value of the grid function u at the point (ξ_j,t_n) is denoted u_j^n. To simplify the notation, we occasionally drop the superscript or subscript on the grid function.

We discretize the spatial operator in (2.2) by the formula

$$\frac{\partial}{\partial\xi}\left(\phi\mu\frac{\partial u}{\partial\xi}\right)\bigg|_{\xi_j}=G(\phi\mu)u_j+\mathcal{O}(h^4),$$

where the fourth order centered operator is given by (here ϕ is absorbed into μ to simplify the notation),

$$G(\mu)u_j:=\frac{1}{12h^2}\big(\bar{\mu}_{j-1}(u_j-u_{j-2})-16\bar{\mu}_{j-1/2}(u_j-u_{j-1})$$
$$+16\bar{\mu}_{j+1/2}(u_{j+1}-u_j)-\bar{\mu}_{j+1}(u_{j+2}-u_j)\big),\qquad j=1,2,\cdots,N_x,\qquad (2.9)$$

and μ is averaged according to

$$\bar{\mu}_j=\frac{1}{2}\big(3\mu_{j-1}-4\mu_j+3\mu_{j+1}\big),\tag{2.10}$$

$$\bar{\mu}_{j+1/2}=\frac{1}{8}\big(\mu_{j-1}+3\mu_j+3\mu_{j+1}+\mu_{j+2}\big).\tag{2.11}$$

In [17], we developed a SBP boundary closure for (2.9). However, only the centered formula is needed here because no physical boundaries are present in the one-dimensional case.

A fourth order accurate time-integration scheme follows from the Taylor expansion

$$\frac{u_j^{n+1}-2u_j^n+u_j^{n-1}}{\Delta_t^2}=u_{tt}|_j^n+\frac{\Delta_t^2}{12}u_{tttt}|_j^n+\mathcal{O}(\Delta_t^4). \tag{2.12}$$

We first consider the domain $x_1 \le \xi \le x_2$, where the super-grid dissipation term is zero because $\sigma=0$. In that case, the semi-discrete approximation of (2.2) gives the formula for the second time derivative of u_j,

$$\rho_j u_{tt}|_j=\phi_j G(\phi\mu)u_j+f(\xi_j,t). \tag{2.13}$$

An expression for the fourth time derivative of u_j follows by differentiating (2.13) twice,

$$\rho_j u_{tttt}|_j=\phi_j G(\phi\mu)u_{tt}|_j+f_{tt}(\xi_j,t). \tag{2.14}$$

Substituting (2.13) and (2.14) into the Taylor series (2.12) gives the fourth order time stepping scheme in the interior of the domain.

When a fourth order ($p=2$) artificial dissipation term is used in (2.2), it is discretized according to

$$(\sigma\rho u_{\xi\xi t})_{\xi\xi}|_j\approx D_+D_-\left(\sigma_j\rho_j D_+D_-\frac{u_j^n-u_j^{n-1}}{\Delta_t}\right)=:Q_4(\sigma\rho)\left(\frac{u_j^n-u_j^{n-1}}{\Delta_t}\right). \tag{2.15}$$

By replacing D_+D_- by $(D_+D_-)^{p/2}$, this formula generalizes to artificial dissipations of order $2p$, for $p=0,2,4,\cdots$.

A sixth order ($p=3$) artificial dissipation term is discretized according to

$$(\sigma\rho u_{\xi\xi\xi t})_{\xi\xi\xi}|_j\approx D_+D_-D_+\left(\sigma_{j-1/2}\rho_{j-1/2}D_-D_+D_-\frac{u_j^n-u_j^{n-1}}{\Delta_t}\right)$$
$$=:Q_6(\sigma\rho)\left(\frac{u_j^n-u_j^{n-1}}{\Delta_t}\right), \tag{2.16}$$

where the average is used for the coefficient, e.g., $\sigma_{j-1/2}=(\sigma_j+\sigma_{j-1})/2$. The above formula can be generalized to any odd $p\ge1$ by replacing the difference operator $D_+D_-D_+$ by $(D_+D_-)^{(p-1)/2}D_+$, and $D_-D_+D_-$ by $D_-(D_+D_-)^{(p-1)/2}$.

Remark 2.1. The discretizations of the dissipation terms are of low order accuracy. However, the coefficient ϵ will later be taken proportional to h^{2p-1}, thereby making these terms artificial in an approximation of the non-dissipative wave equation. With this choice of ϵ, and considering the scheme as an approximation of the non-dissipative wave equation, the dissipation term will restrict the overall accuracy to third order for $p=2$, and to fifth order for $p=3$.

We arrive at the fully discrete approximation of (2.2),

$$\rho_j \frac{u_j^{n+1} - 2u_j^n + u_j^{n-1}}{\Delta_t^2} = \phi_j G(\phi\mu) u_j^n + f(\xi_j, t_n) + \frac{\Delta_t^2}{12} \left(\phi_j G(\phi\mu) \ddot{u}_j^n + f_{tt}(\xi_j, t_n) \right)$$

$$- \varepsilon(-1)^p \phi_j Q_{2p}(\sigma\rho) \left(\frac{u_j^n - u_j^{n-1}}{\Delta_t} \right), \tag{2.17}$$

where

$$\ddot{u}_j^n = (\phi_j G(\phi\mu) u_j^n + f(\xi_j, t_n)) / \rho_j. \tag{2.18}$$

The stencil for $G(\phi\mu)u_j$ in (2.9) is five points wide. If a fourth order dissipation is used, which also is five points wide, we must provide boundary conditions at two ghost points. Three ghost points are needed if a sixth order dissipation is used, because its stencil is seven points wide. In general, we need $\max(2,p)$ boundary conditions.

A natural discretization of the boundary conditions (2.7) is given by

$$B_{sg}(u^n) = (0, \cdots, 0)^T, \quad B_{sg}(\ddot{u}^n) = (0, \cdots, 0)^T, \quad n = 0, 1, 2, \cdots, \tag{2.19}$$

where the boundary operator $B_{sg}(u)$ picks out $\max(2,p)$ ghost point values outside each super-grid boundary,

$$B_{sg}(u) = \left(u_{1-\tilde{p}}, \cdots, u_0, u_{N_x+1}, \cdots, u_{N_x+\tilde{p}} \right)^T, \quad \tilde{p} = \max(2,p). \tag{2.20}$$

Remark 2.2. The implementation of the time-stepping scheme (2.17), (2.18), (2.19) can be simplified by writing it in predictor-corrector form [17]. This formulation also clarifies the application of the boundary conditions during one time step. Given u^n at all interior grid points, the ghost point values of u^n are first defined by enforcing $B_{sg}(u^n) = \mathbf{0}$. We can then evaluate (2.18) to compute $\ddot{u}^n$ at all interior grid points, after which its ghost point values are defined by enforcing $B_{sg}(\ddot{u}^n) = \mathbf{0}$. This defines the corrector term $G(\phi\mu)\ddot{u}^n$ and allows u^{n+1} to be updated at all interior grid points.

2.2 Discrete energy estimate

We begin by defining the one-dimensional discrete L_2 scalar product and norm for real-valued grid functions v_j, w_j, by

$$(v, w)_{h1} = h \sum_{j=1}^{N_x} v_j w_j, \qquad \|v\|_{h1}^2 = (v, v)_{h1}.$$

Essential properties of $G(\phi\mu)u_j$ are specified in the following lemma.

Lemma 2.1. *Let u and v be real-valued grid functions satisfying the boundary condition $B_{sg}(u)=$* **0**, $B_{sg}(v)=$**0**, *and let $\mu_j>0$ and $\phi_j \geq \varepsilon_L >0$ be the grid functions representing the material property and the stretching function, respectively. The spatial operator $G(\phi\mu)$, defined by (2.9), satisfies*

$$(v,Gu)_{h1} = -K_0(v,u) \in \Re, \tag{2.21}$$

where the function $K_0(v,u)$ is bilinear, symmetric and positive definite, i.e., $K_0(v,u) = K_0(u,v)$ and $K_0(u,u) \geq \gamma \|u\|_{h1}^2$, $\gamma>0$.

Proof. See Appendix A.1.   □

The super-grid dissipation term satisfies a similar lemma.

Lemma 2.2. *Let the real-valued grid functions σ and ρ satisfy $\sigma_j \geq 0$ and $\rho_j > 0$. Furthermore, let u and v be real-valued grid functions that satisfy the boundary conditions $B_{sg}(u) = $* **0** *and $B_{sg}(v) = $* **0**. *The super-grid dissipation operator $Q_{2p}(\sigma\rho)$, defined by (2.15) or (2.16), satisfies*

$$(v,Q_{2p}u)_{h1} = (-1)^p C_0(v,u) \in \Re,$$

where the function $C_0(v,u)$ is bilinear, symmetric, and positive semi-definite, i.e., $C_0(v,u) = C_0(u,v)$ and $C_0(u,u) \geq 0$.

Proof. See Appendix A.2.   □

To derive a discrete energy estimate for (2.17), it is convenient to work with grid functions that do not have ghost points. We therefore define grid functions $\bar{u}_j$ and $\bar{v}_j$ such that

$$\bar{u}_j = u_j, \qquad \bar{v}_j = v_j, \qquad 1 \leq j \leq N_x.$$

We also define square matrices K and C_{2p} such that,

$$K_0(u,v) = (\bar{u},K\bar{v})_{h1}, \quad C_0(u,v) = (\bar{u},C_{2p}\bar{v})_{h1}, \quad \text{if } B_{sg}(u) = \mathbf{0} \text{ and } B_{sg}(v) = \mathbf{0}.$$

Because the function $K_0(u,v)$ is symmetric and positive definite, $(\bar{u},K\bar{v})_{h1} = (K\bar{u},\bar{v})_{h1}$ and $(\bar{v},K\bar{v})_{h1} > 0$ for all $\bar{v} \neq 0$, i.e. $K = K^T$ and $K > 0$. From (2.21) we have $(u,Gv)_{h1} = -(\bar{u},K\bar{v})_{h1}$. By taking $u = 0$ except at one interior grid point where $u_j = 1$, we obtain a pointwise identity. The same procedure applies to the damping term Q_{2p}, and we conclude that

$$Gv = -K\bar{v} \quad \text{and} \quad Q_{2p}v = (-1)^p C_{2p}\bar{v}, \quad \text{if } B_{sg}(v) = \mathbf{0}. \tag{2.22}$$

We write the forcing in (2.17) in vector form as $F(t)$, with elements $F_j(t) = f(X(\xi_j),t)$, $j = 1,2,\cdots,N_x$. Also introduce the diagonal matrices M and Φ with elements $M_{jj} = \rho_j$ and $\Phi_{jj} = \phi_j$, respectively. Because the acceleration satisfies the boundary conditions $B_{sg}(\ddot{u}) = $ **0**, there is a grid function without ghost points with elements $\ddot{\bar{u}}_j = \ddot{u}_j$, for $1 \leq j \leq N_x$, such that

$$\ddot{\bar{u}} = -M^{-1}\Phi K\bar{u} + M^{-1}F.$$

We summarize these results in the following Lemma.

Lemma 2.3. *The time-integration scheme (2.17) can be written in matrix form as*

$$\frac{1}{\Delta_t^2} M \left(\bar{u}^{n+1} - 2\bar{u}^n + \bar{u}^{n-1} \right) = -\Phi K \bar{u}^n + F(t^n) + \frac{\Delta_t^2}{12} \left(-\Phi K \ddot{u}^n + F_{tt}(t_n) \right)$$

$$- \frac{\varepsilon}{\Delta_t} \Phi C_{2p} \left(\bar{u}^n - \bar{u}^{n-1} \right), \quad n = 0, 1, 2, \cdots. \tag{2.23}$$

The matrices K and C_{2p}, defined by (2.22), are both symmetric; K is positive definite and C_{2p} is positive semi-definite. The matrices M and Φ are diagonal with positive elements.

The solution of (2.23) is subject to the initial conditions

$$\bar{u}_j^0 = g_0(X(\xi_j)), \qquad \bar{u}_j^{-1} = \tilde{g}_1(X(\xi_j)), \qquad j = 1, 2, \cdots, N_x, \tag{2.24}$$

where $\tilde{g}_1$ depends on g_0 and g_1.

Our main result for the discretization of the one-dimensional wave equation with super-grid layers is formulated in the following theorem.

Theorem 2.1. *Let $\bar{u}^n$, $n = 0, 1, 2, \cdots$, be a solution of the time-integration scheme described in Lemma 2.3. Define the discrete energy by*

$$e^{n+1/2} := \frac{1}{\Delta_t^2} \left(\bar{u}^{n+1} - \bar{u}^n, \Phi^{-1} M(\bar{u}^{n+1} - \bar{u}^n) \right)_{h1} + \left(\bar{u}^{n+1}, K \bar{u}^n - \frac{\Delta_t^2}{12} K M^{-1} \Phi K \bar{u}^n \right)_{h1}$$

$$- \frac{\varepsilon}{2\Delta_t} \left(\bar{u}^{n+1} - \bar{u}^n, C_{2p} \left(\bar{u}^{n+1} - \bar{u}^n \right) \right)_{h1}. \tag{2.25}$$

The discrete energy $e^{n+1/2}$ is a norm of the solution if the inequalities

$$2 \left(\bar{w}, \Phi^{-1} M R_1 \bar{w} \right)_{h1} > \varepsilon \Delta_t \left(\bar{w}, C_{2p} \bar{w} \right)_{h1}, \tag{2.26}$$

$$\left(\bar{w}, \Phi^{-1} M R_2 \bar{w} \right)_{h1} > 0, \tag{2.27}$$

are satisfied for all vectors $\bar{w} \neq 0$. Here, $R_1 = P_1(\Delta_t^2 M^{-1} \Phi K)$ and $R_2 = P_2(\Delta_t^2 M^{-1} \Phi K)$, where P_1 and P_2 are the matrix polynomials,

$$P_1(A) := I - \frac{1}{4} A + \frac{1}{48} A^2, \qquad P_2(A) := \frac{1}{4} A - \frac{1}{48} A^2. \tag{2.28}$$

If $\varepsilon \geq 0$ and $F(t) = 0$, the solution of (2.23) satisfies the energy estimate

$$e^{n+1/2} = e^{n-1/2} - \frac{\varepsilon}{2\Delta_t} \left(\bar{u}^{n+1} - \bar{u}^{n-1}, C_{2p} \left(\bar{u}^{n+1} - \bar{u}^{n-1} \right) \right)_{h1}, \tag{2.29}$$

which is non-increasing in n. The time-stepping scheme (2.23) is therefore stable if the time step satisfies the inequalities (2.26) and (2.27).

Proof. See Appendix A.3.   □

Remark 2.3. In [17] we used the Cayley-Hamilton theorem to analyze the stability of the non-dissipative version of the time-stepping scheme (2.23). When $\varepsilon = 0$ the inequalities (2.26) and (2.27) simplify to eigenvalue conditions, and one can prove that the scheme is stable under the time step restriction

$$\Delta_t \leq \frac{2\sqrt{3}}{\max_j \sqrt{\kappa_j}}, \qquad M^{-1}\Phi K \mathbf{e}_j = \kappa_j \mathbf{e}_j, \qquad \varepsilon = 0.$$

Note that $M^{-1}\Phi K$ has the same spectrum as the symmetric positive definite matrix

$$M^{-1/2}\Phi^{1/2} K \Phi^{1/2} M^{-1/2}.$$

Hence all eigenvalues κ_j are real and positive.

Unfortunately, the energy estimate does not tell us how large the eigenvalues are, and therefore only says that the time-stepping scheme is stable if the time-step is sufficiently small.

2.3   Estimating the time step

In this section we outline how a von Neumann analysis can be used to estimate the stability limit of the time step. For this purpose, we assume constant stretching and dissipation coefficients, as well as constant material properties,

$$\sigma = \sigma_0 \geq 0, \qquad \phi = \phi_0 \geq \varepsilon_L > 0, \qquad \mu = \mu_0 > 0, \qquad \rho = \rho_0 > 0.$$

To study the stability we assume that the external forcing is zero, $f(x,t) = 0$. When all coefficients are constant, the fully discrete scheme (2.17) simplifies to

$$u_j^{n+1} - 2u_j^n + u_j^{n-1} = \frac{\Delta_t^2 \phi_0^2 \mu_0}{\rho_0} \left(D_4 u_j^n + \frac{\Delta_t^2 \phi_0^2 \mu_0}{12\rho_0} (D_4)^2 u_j^n \right)$$
$$- \varepsilon(-1)^p \sigma_0 \phi_0 \Delta_t (D_+ D_-)^p \left(u_j^n - u_j^{n-1} \right), \qquad (2.30)$$

where $D_4 u_j = D_+ D_- u_j - \frac{h^2}{12}(D_+ D_-)^2 u_j$ is a fourth order accurate approximation of $u_{\xi\xi}$.

We start by estimating the stability limit for Δ_t without super-grid dissipation and set $\varepsilon = 0$. After a straightforward von Neumann analysis, we find that the necessary conditions for stability are satisfied if

$$0 \leq \frac{\Delta_t}{h} \sqrt{\frac{\phi_0^2 \mu_0}{\rho_0}} \leq \frac{3}{2}, \qquad \varepsilon = 0. \qquad (2.31)$$

Here, $\sqrt{\phi_0^2 \mu_0/\rho_0}$ is the local phase velocity. When ϕ, μ and ρ vary in space, (2.31) must be satisfied at every point in the domain. Note that the stretching function ϕ reduces the phase velocity in the super-grid layers.

In practice, effects from variable coefficients and boundary conditions can be taken into account by adjusting the coefficient 3/2 on the right hand side of (2.31). Let C_{CFL} denote this adjusted value, which can be determined by numerical experiments. We arrive at the standard CFL-type condition,

$$\frac{\Delta_t}{h} \leq \frac{C_{CFL}}{c_{\max}}, \qquad c_{\max} = \max_{0 \leq \xi \leq x_{\max}} \sqrt{\frac{\mu(\xi)}{\rho(\xi)}}, \qquad \varepsilon = 0. \tag{2.32}$$

Next we study the stability limit inside the super-grid layer, where $\phi \ll 1$ and the local phase velocity is very small. For simplicity we focus on the dissipation term only and consider the stability of

$$u_j^{n+1} - 2u_j^n + u_j^{n-1} = -\varepsilon(-1)^p \sigma_0 \phi_0 \Delta_t (D_+ D_-)^p \left(u_j^n - u_j^{n-1} \right). \tag{2.33}$$

By introducing the un-divided difference operators $\Delta_\pm = hD_\pm$ and the scaled dissipation coefficient

$$\gamma_{2p} = \frac{\varepsilon \Delta_t}{h^{2p}}, \tag{2.34}$$

the simplified scheme (2.33) can be written as

$$u_j^{n+1} - 2u_j^n + u_j^{n-1} = -(-1)^p \gamma_{2p} \sigma_0 \phi_0 (\Delta_+ \Delta_-)^p \left(u_j^n - u_j^{n-1} \right). \tag{2.35}$$

This difference scheme is independent of the grid size and the time step. A von Neumann analysis can be used to show that the necessary conditions for stability of (2.35) are satisfied if

$$0 \leq \gamma_{2p} \sigma_0 \phi_0 \leq \frac{2}{4^p}. \tag{2.36}$$

In practice, we want to use the largest time step that makes the scheme stable without super-grid dissipation, i.e., satisfies (2.32) with equality. The maximum value of the damping coefficient γ_{2p} is then determined by numerical experiments on a coarse grid. Because Δ_t/h satisfies (2.32) with equality, the scaling (2.34) gives

$$\epsilon = \frac{\gamma_{2p} h^{2p}}{\Delta_t} = \frac{\gamma_{2p}}{C} h^{2p-1}, \qquad C := \frac{\Delta_t}{h} = \frac{C_{CFL}}{c_{\max}}, \qquad C = \text{const.} \tag{2.37}$$

An important consequence is that a super-grid dissipation term of order $2p$ introduces an $\mathcal{O}(h^{2p-1})$ perturbation of the original wave equation. Also note that (2.36) indicates that the scaled dissipation coefficient needs to be reduced by a factor 4 when p is increased by one, e.g., when changing from fourth to sixth order super-grid dissipation.

3   The elastic wave equation

This section generalizes the super-grid technique to the half-plane problem for the elastic
wave equation subject to a free surface boundary condition along the physical boundary.
We describe a fourth order accurate discretization that combines SBP-GP operators at the
free surface boundary, centered operators in the interior, and our simplified boundary
closure at the super-grid boundaries. For clarity of presentation, the description and
analysis are done in two space dimensions. It should be straightforward for the reader
to generalize the results to the three-dimensional equations. See, for example, [13] for a
second order accurate discretization of the three-dimensional equations.

   Consider the time-dependent elastic wave equation in the two-dimensional half-plane
$\mathbf{x} = (x,y) \in \Omega = \{-\infty < x < \infty,\, 0 \le y \le \infty\}$, governing the displacement with Cartesian com-
ponents $\mathbf{u} = (u,v)^T$,

$$\rho u_{tt} = ((2\mu + \lambda)u_x + \lambda v_y)_x + (\mu v_x + \mu u_y)_y + f^{(x)},$$
$$\rho v_{tt} = (\mu v_x + \mu u_y)_x + (\lambda u_x + (2\mu + \lambda)v_y)_y + f^{(y)}, \quad \mathbf{x} \in \Omega,\, t \ge 0. \tag{3.1}$$

The heterogeneous isotropic material is characterized by the density $\rho(\mathbf{x}) > 0$, and the
Lamé parameters $\lambda(\mathbf{x})$ and $\mu(\mathbf{x}) > 0$. In the following we assume $\lambda(\mathbf{x}) > 0$. Furthermore,
$(f^{(x)}, f^{(y)})^T$ are the components of the external forcing functions. The displacement is
subject to initial conditions

$$\mathbf{u} = \mathbf{g}_0, \qquad \mathbf{u}_t = \mathbf{g}_1, \qquad \mathbf{x} \in \Omega,\, t = 0, \tag{3.2}$$

where $\mathbf{g}_0$ and $\mathbf{g}_1$ are the initial data. The solution is subject to a normal stress condition
on the physical boundary,

$$\mu(v_x + u_y) = \tau^{(xy)},$$
$$(2\mu + \lambda)v_y + \lambda u_x = \tau^{(yy)}, \qquad -\infty < x < \infty,\, y = 0,\, t \ge 0, \tag{3.3}$$

where $\tau^{(yy)}$ and $\tau^{(xy)}$ are the boundary forcing functions. When $\tau^{(yy)} = \tau^{(xy)} = 0$ this
boundary condition is often called a free surface, or traction free, condition.

   Similar to the one-dimensional case, we want to calculate the solution of (3.1)-(3.3) in
the sub-domain $\mathbf{x} \in \bar{\Omega} = \{x_1 \le x \le x_2,\, 0 \le y \le y_2\}$. The initial data, external forcing, and
boundary forcing functions are assumed to have compact support in $\bar{\Omega}$. We add super-
grid layers of thickness ℓ outside all sides of $\bar{\Omega}$, except $y = 0$. We choose the coordinate
system such that $x_1 - \ell = 0$, $x_2 + \ell = x_{\max}$, $y_2 + \ell = y_{\max}$, and introduce the coordinate trans-
formation (1.1). Because of the physical boundary condition (3.3) along $y = 0$, we use a
stretching function in the η-direction that satisfies $\phi^{(y)} = 1$ for $0 \le \eta \le y_2$. Similar to the
one-dimensional case, $\phi^{(x)} = 1$ for $x_1 \le \xi \le x_2$. See Fig. 2 for a layout of this configuration.

   After transforming the spatial derivatives in (3.1) and adding an artificial dissipation

of order $2p$, we get the elastic wave equation with super-grid layers,

$$\rho u_{tt} = \phi^{(x)}\frac{\partial}{\partial\xi}\left(\phi^{(x)}(2\mu+\lambda)u_\xi + \phi^{(y)}\lambda v_\eta\right) + \phi^{(y)}\frac{\partial}{\partial\eta}\left(\phi^{(x)}\mu v_\xi + \phi^{(y)}\mu u_\eta\right)$$
$$-\epsilon(-1)^p\phi^{(x)}\frac{\partial^p}{\partial\xi^p}\left(\sigma^{(x)}\rho\frac{\partial^p u_t}{\partial\xi^p}\right) - \epsilon(-1)^p\phi^{(y)}\frac{\partial^p}{\partial\eta^p}\left(\sigma^{(y)}\rho\frac{\partial^p u_t}{\partial\eta^p}\right) + f^{(x)}, \qquad (3.4)$$

$$\rho v_{tt} = \phi^{(x)}\frac{\partial}{\partial\xi}\left(\phi^{(x)}\mu v_\xi + \phi^{(y)}\mu u_\eta\right) + \phi^{(y)}\frac{\partial}{\partial\eta}\left(\phi^{(x)}\lambda u_\xi + \phi^{(y)}(2\mu+\lambda)v_\eta\right)$$
$$-\epsilon(-1)^p\phi^{(x)}\frac{\partial^p}{\partial\xi^p}\left(\sigma^{(x)}\rho\frac{\partial^p v_t}{\partial\xi^p}\right) - \epsilon(-1)^p\phi^{(y)}\frac{\partial^p}{\partial\eta^p}\left(\sigma^{(y)}\rho\frac{\partial^p v_t}{\partial\eta^p}\right) + f^{(y)}. \qquad (3.5)$$

Similar to the one-dimensional case, the coefficients in the damping terms are zero inside the domain of interest, i.e., $\sigma^{(x)}(\xi) = 0$ for $x_1 \leq \xi \leq x_2$ and $\sigma^{(y)}(\eta) = 0$ for $0 \leq \eta \leq y_2$. The damping in the ξ-direction is therefore only added in the layers $0 \leq \xi \leq \ell = x_1$ and $x_2 \leq \xi \leq x_2 + \ell = x_{\max}$. In the η-direction, the damping is only added in the layer $y_2 \leq \eta \leq y_2 + \ell = y_{\max}$. In particular, note that there is no damping in the η-direction near the physical boundary.

The normal stress boundary conditions (3.3) are also mapped to computational coordinates using (1.1). Because $\phi^{(y)} = 1$ for $y = \eta = 0$, we get

$$\mu\left(\phi^{(x)}v_\xi + u_\eta\right) = \tau^{(xy)},$$
$$(2\mu+\lambda)v_\eta + \lambda\phi^{(x)}u_\xi = \tau^{(yy)}, \qquad 0 \leq \xi \leq x_{\max}, \ \eta = 0, \ t \geq 0. \qquad (3.6)$$

We proceed by deriving an energy estimate for the solution of (3.4), (3.5), (3.6). Because $\phi^{(x)} \geq \epsilon_L > 0$ and $\phi^{(y)} \geq \epsilon_L > 0$, we define a weighted scalar product and norm for real-valued functions u and v by

$$(u,v)_{2\phi} = \int_0^{y_{\max}}\int_0^{x_{\max}}\frac{u(\xi,\eta)v(\xi,\eta)}{\phi^{(x)}(\xi)\phi^{(y)}(\eta)}d\xi d\eta, \qquad \|u\|_{2\phi}^2 = (u,u)_{2\phi}.$$

Consider the case without external and boundary forcing, i.e., $f^{(x)} = 0$, $f^{(y)} = 0$, $\tau^{(xy)} = 0$ and $\tau^{(yy)} = 0$. The energy estimate is derived by multiplying (3.4) by $u_t/(\phi^{(x)}\phi^{(y)})$, and (3.5) by $v_t/(\phi^{(x)}\phi^{(y)})$. We then add the results together and integrate over the computational domain. After integration by parts we obtain

$$\frac{d}{dt}E_2(t) = -\epsilon\left(\phi^{(x)}\frac{\partial^p u_t}{\partial\xi^p}, \sigma^{(x)}\rho\frac{\partial^p u_t}{\partial\xi^p}\right)_{2\phi} - \epsilon\left(\phi^{(x)}\frac{\partial^p v_t}{\partial\xi^p}, \sigma^{(x)}\rho\frac{\partial^p v_t}{\partial\xi^p}\right)_{2\phi}$$
$$-\epsilon\left(\phi^{(y)}\frac{\partial^p u_t}{\partial\eta^p}, \sigma^{(y)}\rho\frac{\partial^p u_t}{\partial\eta^p}\right)_{2\phi} - \epsilon\left(\phi^{(y)}\frac{\partial^p v_t}{\partial\eta^p}, \sigma^{(y)}\rho\frac{\partial^p v_t}{\partial\eta^p}\right)_{2\phi} + BT_2, \qquad (3.7)$$

where BT_2 is the boundary term. In the stretched coordinates, the elastic energy satisfies

$$
\begin{aligned}
2E_2(t) =& (u_t,\rho u_t)_{2\phi} + (v_t,\rho v_t)_{2\phi} + \left(\phi^{(x)}u_\xi + \phi^{(y)}v_\eta, \lambda\left(\phi^{(x)}u_\xi + \phi^{(y)}v_\eta\right)\right)_{2\phi} \\
&+ \left(\phi^{(x)}v_\xi + \phi^{(y)}u_\eta, \mu\left(\phi^{(x)}v_\xi + \phi^{(y)}u_\eta\right)\right)_{2\phi} + 2\left(\phi^{(x)}u_\xi, \mu\phi^{(x)}u_\xi\right)_{2\phi} \\
&+ 2\left(\phi^{(y)}v_\eta, \mu\phi^{(y)}v_\eta\right)_{2\phi}.
\end{aligned}
\tag{3.8}
$$

Remark 3.1. Similar to the one-dimensional case, the strength of the damping is determined by $\varepsilon\phi^{(x)}\sigma^{(x)}$ in the ξ-direction and by $\varepsilon\phi^{(y)}\sigma^{(y)}$ in the η-direction. The strength is accumulated near corners where two super-grid layers meet.

The boundary term, BT_2, in (3.7) can be evaluated in the same way as was done for the one-dimensional case, in (2.6). Because $\tau^{(xy)} = \tau^{(yy)} = 0$ in boundary condition (3.6), all boundary terms from $\eta = 0$ cancel. The remaining boundary terms in BT_2 become zero if we enforce the boundary conditions

$$
\mathbf{u} = 0, \quad \mathbf{u}_\xi = 0, \cdots, \quad \frac{\partial^{p-1}\mathbf{u}}{\partial\xi^{p-1}} = 0, \quad \xi = \{0, x_{\max}\}, \ 0 \le \eta \le y_{\max}, \ t \ge 0,
\tag{3.9}
$$

and

$$
\mathbf{u} = 0, \quad \mathbf{u}_\eta = 0, \cdots, \quad \frac{\partial^{p-1}\mathbf{u}}{\partial\eta^{p-1}} = 0, \quad 0 \le \xi \le x_{\max}, \ \eta = y_{\max}, \ t \ge 0.
\tag{3.10}
$$

The elastic energy $E_2(t)$ is a norm of $\mathbf{u}$ for all $\mathbf{u}$ that satisfy the homogeneous boundary conditions (3.6), (3.9), and (3.10), because $\rho > 0$, $\lambda > 0$, $\mu > 0$, $\phi^{(x)} \ge \varepsilon_L$, and $\phi^{(y)} \ge \varepsilon_L$, where $\varepsilon_L > 0$.

Remark 3.2. Boundary conditions (3.9) and (3.10) remove the translational and rotational rigid body invariants from $\mathbf{u}$. These invariants would otherwise correspond to motions with zero elastic energy and make $E_2(t)$ a semi-norm, see e.g. [17] for details.

We summarize the results of this section in the following lemma.

Lemma 3.1. *Let* $\mathbf{u} = (u,v)$ *be a solution of the elastic wave equation with super-grid dissipation* (3.4), (3.5), *subject to the boundary conditions* (3.6), (3.9), (3.10). *Let the order of the super-grid dissipation be* $2p$, $p \ge 0$. *Furthermore, assume that the external and boundary forcing functions are zero, i.e.* $f^{(x)} = f^{(y)} = 0$ *and* $\tau^{(xy)} = \tau^{(yy)} = 0$. *Furthermore, assume that the material parameters and the stretching functions satisfy* $\lambda > 0$, $\mu > 0$, $\rho > 0$, $\phi^{(x)} \ge \varepsilon_L$, *and* $\phi^{(y)} \ge \varepsilon_L$, *where* $\varepsilon_L > 0$. *Then, the elastic energy* $E_2(t)$, *defined by* (3.8), *is a norm of the solution and satisfies* (3.7) *with zero boundary term,* $BT_2 = 0$. *If the coefficient of the dissipation satisfies* $\varepsilon \ge 0$, *the right hand side of* (3.7) *is non-positive. Therefore,* $\mathbf{u}$ *satisfies the energy estimate* $E_2(t) \le E_2(0)$, *for* $t > 0$. *Assuming that the solution exists, we conclude that the problem is well-posed.*

3.1   Discretizing the elastic wave equation with super-grid layers

We discretize (3.4), (3.5) on the grid $\xi_i = (i-1)h$, $\eta_j = (j-1)h$, where i and j are integers. The domain sizes and the uniform grid spacing $h > 0$ are defined such that $x_{N_x} = x_{\max}$ and $y_{N_y} = y_{\max}$. Time is discretized on a grid with constant time step, $\Delta_t > 0$. We denote the approximation of the displacement at grid point (x_i, y_j) and time level $t_n = n\Delta_t$ by $\mathbf{u}_{i,j}^n = (u_{i,j}^n, v_{i,j}^n)^T$.

The first two terms on the right hand sides of (3.4) and (3.5) are discretized according to

$$L_h^{(u)}\mathbf{u} = \phi^{(x)}G^{(x)}\left(\phi^{(x)}(2\mu+\lambda)\right)u + \phi^{(x)}D^{(x)}\left(\phi^{(y)}\lambda D^{(y)}v\right) + \phi^{(y)}D^{(y)}\left(\phi^{(x)}\mu D^{(x)}v\right)$$
$$+ \phi^{(y)}G^{(y)}\left(\phi^{(y)}\mu\right)u, \tag{3.11}$$

and

$$L_h^{(v)}\mathbf{u} = \phi^{(x)}G^{(x)}\left(\phi^{(x)}\mu\right)v + \phi^{(x)}D^{(x)}\left(\phi^{(y)}\mu D^{(y)}u\right) + \phi^{(y)}D^{(y)}\left(\phi^{(x)}\lambda D^{(x)}u\right)$$
$$+ \phi^{(y)}G^{(y)}\left(\phi^{(y)}(2\mu+\lambda)\right)v, \tag{3.12}$$

respectively. Here, the grid indices on the grid functions are suppressed to simplify the notation. On vector notation, the discretization is denoted

$$\mathbf{L}_h\mathbf{u}_{i,j}^n = \begin{pmatrix} L_h^{(u)}\mathbf{u}_{i,j}^n \\ L_h^{(v)}\mathbf{u}_{i,j}^n \end{pmatrix}.$$

The finite difference operators $G^{(x)}$ and $D^{(x)}$ in the above formulas act along the first index (ξ-direction). The fourth order accurate operator $G^{(x)}(\mu)w_{i,j}$ approximates $(\mu w_\xi)_\xi(\xi_i, \eta_j)$. Besides operating on a two-dimensional grid function, it is the same as the one-dimensional operator G in (2.9). The difference operator $D^{(x)}w_{i,j}$ is a fourth order accurate centered approximation of $w_\xi(\xi_i, \eta_j)$. It can be written

$$D^{(x)}w_{i,j} := D_{0x}w_{i,j} - \frac{h^2}{6}D_{0x}D_{+x}D_{-x}w_{i,j} = \frac{1}{12h}\left(-w_{i+2,j} + 8w_{i+1,j} - 8w_{i-1,j} + w_{i-2,j}\right),$$
$$D_{0x} = \frac{1}{2}(D_{+x} + D_{-x}). \tag{3.13}$$

Note that the difference operators $G^{(x)}$ and $D^{(x)}$ are *not* boundary modified and do *not* satisfy standard SBP properties. As in the one-dimensional case, two ghost points are needed outside the super-grid boundaries $\xi = 0$ and $\xi = x_{\max}$.

The fourth order accurate finite difference operators $G^{(y)}(\phi^{(y)}\mu)u$ and $D^{(y)}u$ approximate $(\phi^{(y)}\mu u_\eta)_\eta$ and u_η, respectively. These are one-dimensional operators acting along the second index (η-direction), but with SBP-GP boundary modifications at the $\eta = 0$

boundary, as described in [17]. For this reason, one ghost point is needed outside the physical boundary $\eta=0$, and two ghost points are needed outside the super-grid boundary $\eta=y_{\max}$, where there is no boundary modification.

The artificial dissipation operators in (3.4) and (3.5) are discretized in the same way as in the one-dimensional case. The dissipation of order $2p$ is denoted by $Q_{2p}^{(x)}$ in the ξ-direction and $Q_{2p}^{(y)}$ in the η-direction. On vector form, the two-dimensional dissipation becomes

$$\mathbf{Q}_{2p}\mathbf{u}=\begin{pmatrix}\phi^{(x)}Q_{2p}^{(x)}(\sigma^{(x)}\rho)u+\phi^{(y)}Q_{2p}^{(y)}(\sigma^{(y)}\rho)u\\\phi^{(x)}Q_{2p}^{(x)}(\sigma^{(x)}\rho)v+\phi^{(y)}Q_{2p}^{(y)}(\sigma^{(y)}\rho)v\end{pmatrix}. \tag{3.14}$$

The dissipation requires p ghost points outside each super-grid boundary. Note that the dissipation in the y-direction does not need any ghostpoints outside $\eta=0$, because the dissipation coefficient is zero near this boundary, i.e. $\sigma^{(y)}=0$.

The normal stress boundary conditions (3.6) are discretized by the fourth order accurate formulas

$$\mu_{i,1}\left(B^{(y)}u_{i,1}+\phi_i^{(x)}D^{(x)}v_{i,1}\right)=\tau_i^{(xy)}, \tag{3.15}$$

$$(2\mu+\lambda)_{i,1}B^{(y)}v_{i,1}+\lambda_{i,1}\phi_i^{(x)}D^{(x)}u_{i,1}=\tau_i^{(yy)}, \tag{3.16}$$

for $1\le i\le N_x$. The boundary operator $B^{(y)}v_{i,1}$ is derived in [17]. It is a fourth order accurate approximation of $v_y(x_i,y_1)$ of the form $\sum_{l=0}^4 c_l v_{i,l}$, where $c_0\ne 0$. Therefore, (3.15) and (3.16) can be solved for the ghost point values $u_{i,0}$ and $v_{i,0}$.

We define the following boundary operators for two-dimensional grid functions,

$$B_{sg1}(\mathbf{u}):=\left(\mathbf{u}_{1-\tilde{p},j},\cdots,\mathbf{u}_{0,j},\mathbf{u}_{N_x+1,j},\cdots,\mathbf{u}_{N_x+\tilde{p},j}\right)^T, \quad 1-\tilde{p}\le j\le N_y+\tilde{p}, \tag{3.17}$$

$$B_{sg2}(\mathbf{u}):=\left(\mathbf{u}_{i,N_y+1},\cdots,\mathbf{u}_{i,N_y+\tilde{p}}\right)^T, \quad 1-\tilde{p}\le i\le N_x+\tilde{p}. \tag{3.18}$$

As in the one-dimensional case, $\tilde{p}=\max(2,p)$. The boundary conditions (3.9) and (3.10) are discretized by

$$B_{sg1}(\mathbf{u})=(0,\cdots,0)^T, \qquad B_{sg2}(\mathbf{u})=(0,\cdots,0)^T. \tag{3.19}$$

Using the above notation and the same time discretization as in Section 2.1, we can write the finite difference approximation of the elastic wave equation with super-grid layers on vector form,

$$\rho\frac{\mathbf{u}^{n+1}-2\mathbf{u}^n+\mathbf{u}^{n-1}}{\Delta_t^2}=\mathbf{L}_h\mathbf{u}^n+\mathbf{f}^n+\frac{\Delta_t^2}{12}\left(\mathbf{L}_h\ddot{\mathbf{u}}^n+\mathbf{f}_{tt}^n\right)-\varepsilon(-1)^p\mathbf{Q}_{2p}\left(\frac{\mathbf{u}_{i,j}^n-\mathbf{u}_{i,j}^{n-1}}{\Delta_t}\right), \tag{3.20}$$

where $\mathbf{u}^n=(u^n,v^n)^T$ is subject to the normal stress boundary conditions (3.15), (3.16) as well as the Dirichlet conditions $B_{sg1}(\mathbf{u}^n)=\mathbf{0}$ and $B_{sg2}(\mathbf{u}^n)=\mathbf{0}$. In (3.20), the acceleration is defined by

$$\ddot{\mathbf{u}}_{i,j}^n=\left(\mathbf{L}_h\mathbf{u}_{i,j}^n+\mathbf{f}_{i,j}^n\right)/\rho_{i,j}, \qquad 1\le i\le N_x, 1\le j\le N_y, \tag{3.21}$$

which is subject to the Dirichlet conditions $B_{sg1}(\ddot{\mathbf{u}}^n) = \mathbf{0}$ and $B_{sg2}(\ddot{\mathbf{u}}^n) = \mathbf{0}$. It is also subject to the normal stress conditions (3.15), (3.16), where the boundary forcing functions $(\tau^{(xy)}, \tau^{(yy)})$ are replaced by their second time derivatives.

3.2 Energy estimate

In our previous work for second and fourth order accurate methods, e.g., [13, 17], the discrete energy estimate is derived based on the fundamental property

$$(\mathbf{w}, \mathbf{L}_h \mathbf{u})_{hw} = -S_h(\mathbf{w}, \mathbf{u}) + T_h(\mathbf{w}, \mathbf{u}). \tag{3.22}$$

Here, $(\mathbf{u}, \mathbf{v})_{hw}$ is a weighted scalar product and the bilinear form $S_h(\mathbf{w}, \mathbf{u})$ is symmetric and positive semi-definite. The term $T_h(\mathbf{w}, \mathbf{u})$ is also bilinear and consists of contributions from the boundary. In particular, $T_h(\mathbf{w}, \mathbf{u}) = 0$ when $\mathbf{w}$ satisfies homogeneous Dirichlet conditions, or $\mathbf{u}$ satisfies free surface conditions, see [13, 17] for details.

Our previous estimates hold when the difference operators in $\mathbf{L}_h \mathbf{u}$ are SBP modified at all boundaries of the domain, and when the scalar product is correspondingly weighted near all boundaries. We proceed by proving that the fundamental relation (3.22) also holds without SBP modifications near the super-grid boundaries. Define the weighted scalar product for real-valued scalar grid functions $u_{i,j}$ and $v_{i,j}$ by

$$(u, v)_{hw} = h^2 \sum_{j=1}^{N_y} \sum_{i=1}^{N_x} \omega_j u_{i,j} v_{i,j}.$$

The corresponding scalar product for real valued vector grid functions $\mathbf{u}_{i,j}$ and $\mathbf{v}_{i,j}$, is

$$(\mathbf{u}, \mathbf{v})_{hw} = \left(u^{(x)}, v^{(x)}\right)_{hw} + \left(u^{(y)}, v^{(y)}\right)_{hw}, \qquad \mathbf{u} = \begin{pmatrix} u^{(x)} \\ u^{(y)} \end{pmatrix}, \qquad \mathbf{v} = \begin{pmatrix} v^{(x)} \\ v^{(y)} \end{pmatrix}.$$

Because the difference operators are SBP modified only at the boundary $\eta = 0$, the weight in the scalar product, ω_j, only depends on j. Furthermore, it is only different from unity for $1 \le j \le 4$.

To handle the relation between cross-terms and second derivatives, we need to show that $D^{(x)} u$ is anti-symmetric.

Lemma 3.2. *Let $u_{i,j}$ and $v_{i,j}$ be real-valued grid functions satisfying the boundary conditions $B_{sg1}(u) = \mathbf{0}$ and $B_{sg1}(v) = \mathbf{0}$. Let $D^{(x)}$ denote the finite difference operator defined by (3.13). Then,*

$$\left(v, D^{(x)} u\right)_{hw} = -\left(D^{(x)} v, u\right)_{hw}.$$

Proof. See Appendix A.4.   □

To prove an energy estimate for the two-dimensional spatial discretization (3.20) together with boundary conditions (3.15), (3.16), and (3.19), we proceed as follows. We first apply Lemmas 2.1, 2.2, and 3.2, on each operator in the x-direction. For the operators in the y-direction, Lemmas 2.1, 2.2, and 3.2 are modified by the summation by parts boundary terms at $\eta = 0$, and become

$$\left(v, G^{(y)}(\mu)u\right)_{hw} = -K_0^{(y)}(v,u) - h\sum_{i=1}^{N_x} \mu_{i,1}v_{i,1}B^{(y)}u_{i,1}, \tag{3.23}$$

$$\left(v, D^{(y)}u\right)_{hw} = -\left(D^{(y)}v,u\right)_{hw} - h\sum_{i=1}^{N_x} u_{i,1}v_{i,1}, \tag{3.24}$$

$$\left(v, Q_h^{(y)}u\right)_{hw} = C_0^{(y)}(v,u). \tag{3.25}$$

Here, the function $K_0^{(y)}(v,u)$ contains a sum of one-dimensional functions $K_0(v,u)$, which is defined in Lemma 2.1. Similarly, the function $C_0^{(y)}(v,u)$ contains a sum of one-dimensional functions $C_0(v,u)$, which is defined in Lemma 2.2. The super-grid dissipation operator $Q_h^{(y)}$ gives no contributions to the boundary terms at $\eta = 0$, because $\sigma^{(y)}$ is zero there.

Corresponding to lemmas 2.1 and 2.2 in the one-dimensional case, the essential properties of the two-dimensional spatial discretization are specified in the following theorem.

Theorem 3.1. *Let $\mathbf{u}_{i,j}$ and $\mathbf{w}_{i,j}$ be grid functions that satisfy the boundary conditions (3.15), (3.16), and (3.19). The fourth order spatial operators (3.11), (3.12) then satisfy*

$$\left(\mathbf{w}, \frac{1}{\phi^{(x)}\phi^{(y)}}\mathbf{L}_h\mathbf{u}\right)_{hw} = -S_h(\mathbf{w},\mathbf{u}), \tag{3.26}$$

where S_h is bilinear, symmetric, and positive definite. Furthermore, the dissipation operator (3.14) satisfies

$$\left(\mathbf{w}, \frac{1}{\phi^{(x)}\phi^{(y)}}\mathbf{Q}_{2p}\mathbf{u}\right)_{hw} = C_h(\mathbf{w},\mathbf{u}),$$

where C_h is bilinear, symmetric, and positive semi-definite.

Proof. See Appendix A.5. □

The discretization of the elastic wave equation with super-grid layers, (3.20), can be written in matrix form as (2.23), with symmetric positive (semi-)definite matrices K and C_{2p}. Similar to the one-dimensional case, these matrices are defined through $S_h(\mathbf{w},\mathbf{u}) = \mathbf{w}^T K \mathbf{u}$ and $C_h(\mathbf{w},\mathbf{u}) = \mathbf{w}^T C_{2p}\mathbf{u}$. Furthermore, in the two-dimensional case, the matrix Φ is still diagonal, with elements $\phi^{(x)}\phi^{(y)}$. For example,

$$\mathbf{L}_h\mathbf{u} = \phi^{(x)}\phi^{(y)}\left(\frac{1}{\phi^{(x)}\phi^{(y)}}\mathbf{L}_h\mathbf{u}\right) = -\phi^{(x)}\phi^{(y)}K\mathbf{u} = -\Phi K\mathbf{u}.$$

The remaining terms in (3.20) can be rewritten similarly, allowing the finite difference scheme for the elastic wave equation to be cast in the same matrix formulation as the scalar wave equation, i.e., (2.23). Theorem 2.1 therefore applies also to (3.20), and we obtain our main result.

Theorem 3.2. *The finite difference scheme* (3.20) *with zero forcing* $\mathbf{f}^n = 0$ *and homogeneous boundary conditions* (3.15), (3.16), *and* (3.19), *has a non-increasing discrete energy*

$$e^{n+1/2} \leq e^{n-1/2} \leq \cdots \leq e^{1/2}.$$

The discrete energy, corresponding to (2.25), *is a norm of the solution when the time step satisfies the inequalities corresponding to* (2.26) *and* (2.27). *Therefore, the scheme* (3.20) *is stable.*

3.3 Time step restriction in several space dimensions

Similar to the one-dimensional wave equation, a von Neumann analysis can be used to estimate the stability limit of the time step for the two-dimensional elastic wave equation. Here we will only study the influence of the super-grid dissipation in the fully discretized elastic wave equation and therefore take $\mathbf{L}=0$ in (3.20). After assuming zero forcing, constant stretching and dissipation coefficients as well as material properties, the dissipative terms in (3.20) become

$$\frac{\mathbf{u}^{n+1}-2\mathbf{u}^n+\mathbf{u}^{n-1}}{\Delta_t^2} = -\varepsilon(-1)^p \left[\phi_0^{(x)}\sigma_0^{(x)}(D_+^\xi D_-^\xi)^p + \phi_0^{(y)}\sigma_0^{(y)}(D_+^\eta D_-^\eta)^p \right] \left(\frac{\mathbf{u}^n-\mathbf{u}^{n-1}}{\Delta_t} \right).$$

To perform the von Neumann analysis, we assume that the solution is 2π-periodic in ξ and η, and expand the solution in a Fourier series. After some algebra, the necessary condition for stability becomes

$$0 \leq \gamma_{2p} \left(\phi_0^{(x)}\sigma_0^{(x)} + \phi_0^{(y)}\sigma_0^{(y)} \right) \leq \frac{2}{4^p},$$

where γ_{2p} is the scaled dissipation coefficient defined by (2.34). On sides away from corners, either $\sigma^{(x)}=0$ or $\sigma^{(y)}=0$. However, both $\sigma^{(x)}$ and $\sigma^{(y)}$ are positive in the corner regions, where two super-grid layers meet.

To avoid having to significantly reduce γ_{2p} compared to the one-dimensional case, it is necessary to reduce $\sigma^{(x)}$ and $\sigma^{(y)}$ near the corners. A simple solution is provided by introducing a linear taper function. For example, in the corner region $0 \leq \xi \leq x_1, 0 \leq \eta \leq y_1$, we define

$$\tau(x) = \begin{cases} \alpha, & x<0, \\ \alpha+(1-\alpha)x/\ell, & 0 \leq x \leq \ell, \\ 1, & x>\ell. \end{cases}$$

We take $\alpha=1/3$ and define the two-dimensional damping functions by

$$\sigma^{(x)}(\xi,\eta)=\tau(\eta)\sigma(\xi), \qquad \sigma^{(y)}(\xi,\eta)=\tau(\xi)\sigma(\eta),$$

where $\sigma(x)$ is the one-dimensional damping function (2.5). Using this construction, the strength of the damping is determined by

$$I_2(\xi,\eta) := \phi^{(x)}\sigma^{(x)} + \phi^{(y)}\sigma^{(y)} = \tau(\eta)\psi(\xi) + \tau(\xi)\psi(\eta),$$

where $\psi(x)$ is the auxiliary function (2.4). This construction satisfies $\max I_2 = 1$. Away from the corner, the strength of the damping is the same as in the one-dimensional case because $\psi(x)=0$ and $\tau(x)=1$ for $x \geq \ell$. Therefore, $I_2(\xi,\eta)=\psi(\eta)$ for $\xi \geq \ell$ and $I(\xi,\eta)=\psi(\xi)$ for $\eta \geq \ell$. At the corner, $\tau(0)=1/3$ and $\psi(0)=1$, giving $I_2(0,0)=2/3$. The function $I_2(\xi,\eta)$ has a local maxima along the diagonal $\xi=\eta \approx 0.31\ell$, where $I_2 \approx 0.983$. The tapering approach is straight forward to generalize to the other corners of the computational domain.

In three dimensions, the strength of the damping equals $I_3 := \phi^{(x)}\sigma^{(x)} + \phi^{(y)}\sigma^{(y)} + \phi^{(z)}\sigma^{(z)}$. We generalize the tapering approach by defining $\sigma^{(x)}(\xi,\eta,\zeta) = \tau(\eta)\tau(\zeta)\sigma(\xi)$, etc. This construction also satisfies $\max I_3 = 1$. Note that the two-dimensional strength is recovered along edges of the three-dimensional domain (where two super-grid layers meet), because $I_3(\xi,\eta,\zeta) = I_2(\xi,\eta)$ for $\zeta \geq \ell$, etc. In corners where three supergrid layers meet, the strength of the damping has a local maxima along the space-diagonal $\xi=\eta=\zeta \approx 0.37\ell$ where $I_3 \approx 0.823$.

The tapering approach is of significant practical importance in three-dimensional calculations, where up to three super-grid layers can meet at corners. This is because the tapering keeps the maximum strength of the super-grid damping approximately the same along sides, edges, and corners of the computational domain. Let γ_{2p} be the damping coefficient that makes the time stepping stable in the case with super-grid damping in only one direction. With the tapering approach, this value will also work when three super-grid layers meet at a corner. Without the tapering approach, the time stepping would become unstable unless the damping coefficient is reduced to approximately $\gamma_{2p}/3$. Because the maximum strength of the damping is reduced by a factor of three along the sides of the domain (where only one super-grid damping term is active), the layers would need to be approximately three times thicker to damp out the solution to the same level. Since the super-grid layers are added outside the domain of interest, tripling their thickness would significantly increase the total number of grid points in a three-dimensional case, and make the calculation much more expensive.

4   Numerical experiments

All simulations reported here were performed with the open source code SW4, version 1.0 [15], which solves the three-dimensional elastic wave equation on parallel computers. This code implements the three-dimensional version of the numerical methods described in the previous sections, which satisfy corresponding stability and accuracy results. In all numerical experiments, the order of the super-grid dissipation operator will be either 4 or 6, and the threshold value for the super-grid stretching functions is set to $\varepsilon_L = 10^{-4}$. All calculations use a box-shaped computational domain $(x,y,z) \in [0,x_{\max}] \times [0,y_{\max}] \times$

$[0,z_{\max}]$. A free surface boundary condition is imposed along $z=0$ and super-grid layers are included on all other sides of the domain.

4.1 Lamb's problem

Lamb [8] derived an analytic solution of the elastic wave equation in a homogeneous half-space, subject to an impulsive vertical point forcing applied on the free surface boundary. Many generalizations have been made to Lamb's original derivation, see for example [11] or [5]. Here we focus on the case with $\lambda=\mu$ (Poisson ratio 1/4) where the evaluation of the analytic solution is somewhat simplified.

We shall solve Lamb's problem numerically and take the domain of interest to be $\ell\leq x\leq 8+\ell$, $\ell\leq y\leq 8+\ell$, $0\leq z\leq 4+\ell$. The forcing is given by the singular point force

$$\mathbf{f}(\mathbf{x},t)=\begin{pmatrix} 0 \\ 0 \\ g(t)\delta(\mathbf{x}-\mathbf{x}_0) \end{pmatrix},$$

where $\delta(\mathbf{x}-\mathbf{x}_0)$ is the Dirac distribution centered at $\mathbf{x}_0=(4+\ell,4+\ell,0)$. The point force is discretized in space by using the technique described in [14]. The time function satisfies

$$g(t)=\begin{cases} 16384t^7(1-t)^7, & 0<t<1, \\ 0, & \text{otherwise.} \end{cases} \tag{4.1}$$

The source time function $g(t)$ is six times continuously differentiable, symmetric around $t=0.5$, where $g(0.5)=1$. The smoothness in time of the point forcing translates to smoothness in space of the solution after the point force has stopped acting, i.e., for times $t>1$. Super-grid layers of width ℓ are added to all sides of the domain of interest, except along $z=0$, where homogeneous free surface conditions corresponding to (3.15) and (3.16) are imposed. We choose the units such that the homogeneous elastic material has the properties $\mu=\lambda=\rho=1$. The computational domain is taken to be $0\leq x\leq 8+2\ell=:x_{\max}$, $0\leq y\leq 8+2\ell=:y_{\max}$, $0\leq z\leq 4+\ell=:z_{\max}$.

Fig. 3 shows the numerical solution at three different times when the super-grid layer has thickness $\ell=2$, the grid size is $h=0.02$, and the fourth order damping coefficient is $\gamma_4=0.02$. Here the magnitude of the displacement, $\sqrt{u^2+v^2+w^2}$, is plotted. The top left and right subfigures show a strong Rayleigh surface wave, a shear wave, and the remnants of a weak compressional wave. In this material, the shear wave moves outwards with phase velocity $c_s=1$ and the compressional wave has phase velocity $c_p=\sqrt{3}$. For a material with $\mu=\lambda=1$ it can be shown that the Rayleigh surface wave propagates with phase velocity $c_r\approx 0.92$. Because the wave speed in each direction of the super-grid layers is proportional to the value of the corresponding stretching function, the solution slows down and becomes compressed inside the super-grid layers. Also note that the wave fronts tend towards a square shape as time progresses. We remark that no artificially
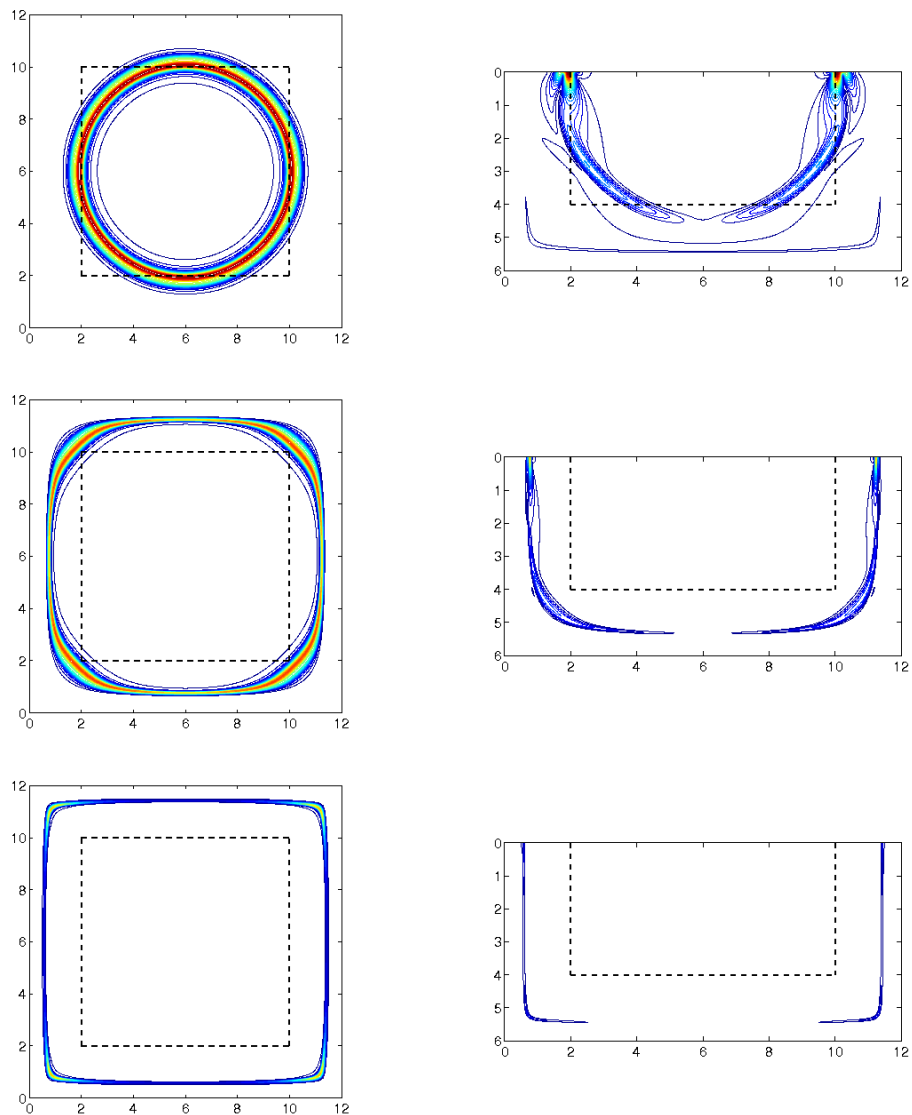
Figure 3: Magnitude of the displacement for Lamb's problem at times 5, 7, and 9 (top to bottom) in the $z\!=\!0$ plane (left) and the $x\!=\!6$ plane (right). The super-grid layers are outlined by a dashed line and have thickness $\ell\!=\!2$. The contour levels are the same in all plots and are spaced between 0.01 (dark blue) and 0.26 (red) with step size 0.01.

reflected waves are visible within the domain of interest, here outlined with a dashed line.

Mooney [11] gives explicit expressions for the analytical solution of Lamb's problem on the surface $z\!=\!0$ in terms of a Green's function, $G(t)$. The z-component of the solution

at a point on the surface satisfies

$$w(x,y,0,t) = \frac{K}{r} \int_0^t g'(t-\tau) G\left(\frac{\tau}{r}\right) d\tau, \tag{4.2}$$

where $r = \sqrt{x^2 + y^2}$, and

$$G(\xi) = \begin{cases} 0, & \xi < 1/\sqrt{3}, \\ c_1 + c_2/\sqrt{\gamma^2 - \xi^2} + c_3/\sqrt{\xi^2 - b^2} + c_4/\sqrt{\xi^2 - 1/4}, & 1/\sqrt{3} < \xi < 1, \\ c_5 + c_6/\sqrt{\gamma^2 - \xi^2}, & 1 < \xi < \gamma, \\ c_7, & \gamma < \xi. \end{cases} \tag{4.3}$$

The values of the constants K, c_i, b, and γ are given in [11], with $b \approx 0.563$ and $\gamma \approx 1.0877$. Hence all integrands are non-singular, except in the third case of (4.3), which has an integrable singularity at $\xi = \gamma$. When g is given by (4.1), we obtain the exact solution as a sum of terms that either are integrals of polynomials, or have the form

$$\int \frac{P(\xi)}{\sqrt{\xi^2 - a^2}} d\xi. \tag{4.4}$$

where $P(\xi)$ is a polynomial in ξ. Analytical expressions for integrals of the form (4.4) can be found, but their numerical evaluation is very sensitive to round-off errors, due to the high polynomial order of P. These analytical formulas are therefore inadequate for numerically calculating the exact solution. Instead, we numerically evaluate the convolution integral (4.2) using the Quadpack library from the Netlib repository [12]. This approach turns out to be much better conditioned, and permits us to evaluate the formula (4.2) to within approximately 12 decimal places.

Because the analytical solution is only available along the surface ($z = 0$), we study the accuracy of the numerical solution along the surface of the domain of interest, i.e., for $z = 0$, inside the super-grid layers: $\ell \le x \le x_{\max} - \ell$, $\ell \le y \le y_{\max} - \ell$.

As can be seen in Fig. 3, the solution is dominated by shear and surface waves. The distance between the point force and the closest super-grid layer equals 4, so the shear waves start arriving at the super-grid layer at time $t = 4$. They leave the surface of the domain of interest at time $t = 1 + 4\sqrt{2} \approx 6.65$. The slowest wave in the solution is the surface wave, propagating at phase velocity $c_r \approx 0.92$. The surface waves therefore leave the domain of interest around $t \approx 1 + 4\sqrt{2}/0.92 \approx 7.15$. After that time, the exact solution is zero along the surface of the domain of interest.

Fig. 4 shows the L_2 norm of the error in the w-component of the solution, as function of time. The norm is evaluated over the surface of the domain of interest. Note that the point force makes the exact solution unbounded at $\mathbf{x} = \mathbf{x}_0$ for $0 < t < 1$, making the norm of the error undefined. A few grid points near $\mathbf{x}_0$ are therefore excluded from the norm calculation. The errors corresponding to grid sizes $h = 0.04$ (blue), $h = 0.02$ (red), and $h = 0.01$ (black) are shown in Fig. 4. Three different regimes of the error can be
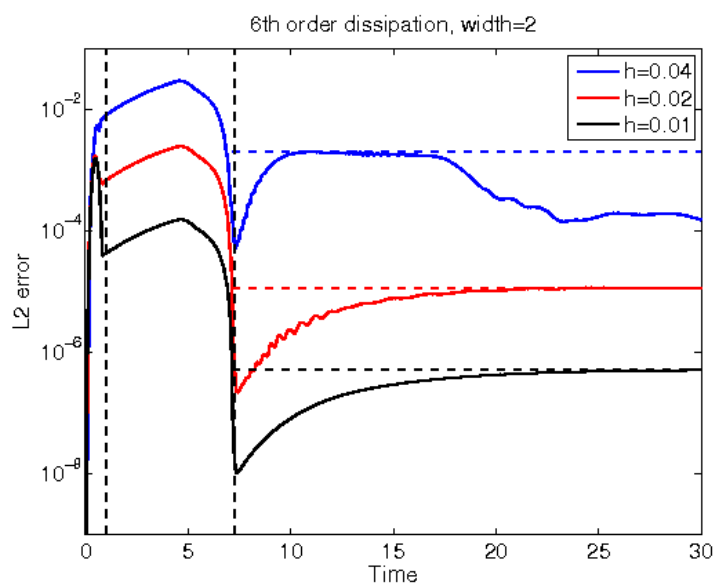
Figure 4: L_2 error in the vertical component of Lamb's problem with sixth order artificial dissipation for grid sizes $h=0.04$ (blue), $h=0.02$ (red), and $h=0.01$ (black). The width of the super-grid layer is $\ell=2$. The dashed vertical lines indicate times $t=1$ and $t=7.15$. The dashed horizontal lines indicate the max errors in time for $t>7.5$.

distinguished. First, for $0<t<1$, the point force is active and the numerical solution has a large error near $\mathbf{x}_0$, where the exact solution is unbounded. No reduction of the norm of the error is obtained as the grid is refined. Then follows a time interval where the error first increases and then decreases, i.e., $1\leq t\leq 7.15$. Here the forcing is zero and the solution error is dominated by propagation errors. Note that the L_2-norm of the error is reduced by approximately a factor of 16 each time the grid size is halved, indicating a fourth order convergence rate. The reason the error decays between $t\approx 5$ and $t\approx 7.15$ is because the shear and surface waves are leaving the domain of interest. Artificial reflections from the super-grid layers become noticeable around $t\approx 7.5$ and we take the third interval to be $t>7.5$. The simulations are run to time 30.

To investigate the amount of artificial reflections from the super-grid layers, we study the maximum value of the L_2 errors for times $7.5<t\leq 30$, see Table 1. Here the width of the layer, $\ell=N_{SG}h$, is varied as well as the order of the artificial dissipation. The coefficients for the fourth and six order dissipations are $\gamma_4=0.02$ and $\gamma_6=0.005$, except for the first entry ($N_{SG}=13$, $h=0.04$), where those values lead to numerical instabilities. In this case, stability was regained by reducing the coefficients to $\gamma_4=0.01$ and $\gamma_6=0.002$, respectively.

The amount of artificial reflections depends strongly on the width of the super-grid layer, ℓ. On the coarsest grid ($h=0.04$), the fourth order dissipation gives slightly smaller errors than the sixth order dissipation for all widths. However, the sixth order dissipation shows superior performance as the grid is refined. Reflected waves propagate from the layer back into the domain of interest. Because the fourth order dissipation adds a

Table 1: The maximum value of the L_2-norm of the error for times $7.5 < t \leq 30$.

Width	N_{SG}	h	4th order diss.		6th order diss.	
			max error	ratio	max error	ratio
0.52	13	0.04	1.31e-1	–	1.50e-1	–
0.5	25	0.02	3.33-2	3.93	2.08e-2	7.21
0.5	50	0.01	8.51e-3	3.91	2.04e-3	10.20
1	25	0.04	1.91e-2	–	2.33e-2	–
1	50	0.02	2.73e-3	6.98	8.89e-4	26.14
1	100	0.01	4.88e-4	5.60	4.56e-5	19.48
2	50	0.04	1.13e-3	–	1.97e-3	–
2	100	0.02	1.33e-4	8.49	1.16e-5	170.3
2	200	0.01	1.85e-5	7.17	5.09e-7	22.81

third order perturbation to the elastic wave equation, we can only expect the artificial reflections to decay as $\mathcal{O}(h^3)$ when the fourth order dissipation is used. Based on the same argument, the sixth order dissipation should result in a fifth order perturbation of the elastic wave equation. Because the interior scheme is fourth order accurate, the overall convergence rate should be $\mathcal{O}(h^4)$. Except for the thinnest super-grid layer, the results in Table 1 indicate almost third order convergence for the fourth order dissipation and better than fourth order convergence for the sixth order dissipation.

It is also instructive to compare the sizes of the propagation errors with the reflection errors. In our setup, the propagation error can be quantified as the max value of the L_2 norm of the error during the time interval $1 \leq t \leq 7.5$. Evaluating the errors in the numerical solution (here denoted by w_h) gives

$$\max_{1 \leq t \leq 7.5} \|w(\cdot,\cdot,0,t) - w_h(\cdot,\cdot,0,t)\|_2 \approx \begin{cases} 2.95 \cdot 10^{-2}, & h = 0.04, \\ 2.47 \cdot 10^{-3}, & h = 0.02, \\ 1.54 \cdot 10^{-4}, & h = 0.01. \end{cases}$$

As a minimum requirement, we want the reflection errors from the super-grid layers to be smaller than the propagation errors. While this criteria is satisfied for $\ell = 1$ and $\ell = 2$, it is not satisfied for the thinnest super-grid layer ($\ell = 0.5$). Note that the dominant wave length of the solution is approximately one. Our conjecture is that the super-grid layers need to be at least as wide as this wave length.

It is also interesting to study what happens if a fixed number of grid points are used in the super-grid layer. This means that the width of the layer ℓ becomes smaller as the grid is refined. In Table 1, 50 grid points are used in the layer on line 7 ($h = 0.04$), line 5 ($h = 0.02$) and line 3 ($h = 0.01$). When the fourth order dissipation is used, the error grows monotonically as the grid size is decreased. The results for the sixth order dissipation are only marginally better. Here the error is about the same for $h = 0.04$ and $h = 0.01$, but
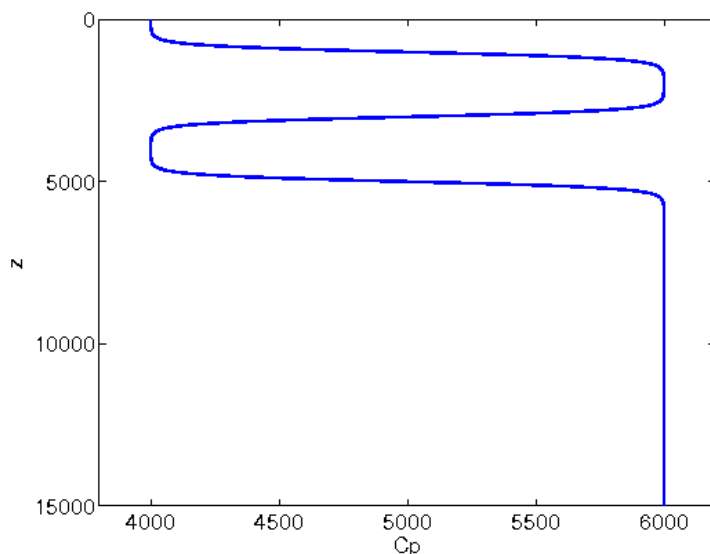
Figure 5: Compressional velocity (c_p) as function of depth (z) in the vertically layered material.

smaller for $h = 0.02$. We conclude that keeping a fixed number of grid points in the layer leads to a modeling error that does not diminish as the grid size tends to zero.

4.2   A heterogeneous half-space problem with smooth material

To further test the reflection properties of the super-grid approach, we consider a regularized layered material model, where c_p, c_s, and ρ depend on z. We let the compressional wave speed vary between $c_p^{(1)} = 4000$ and $c_p^{(2)} = 6000$,

$$
c_p(z) = c_p^{(1)} + \frac{c_p^{(2)} - c_p^{(1)}}{2} \left(1 + \tanh \frac{z - z_1}{L_z} \right) + \frac{c_p^{(1)} - c_p^{(2)}}{2} \left(1 + \tanh \frac{z - z_2}{L_z} \right)
$$
$$
+ \frac{c_p^{(2)} - c_p^{(1)}}{2} \left(1 + \tanh \frac{z - z_3}{L_z} \right).
$$

The transition points are $z_1 = 1000$, $z_2 = 3000$, $z_3 = 5000$, and the transition length scale is $L_z = 200$. The resulting function is plotted in Fig. 5. The shear speed and density vary in a corresponding way with $c_s^{(1)} = 2000$, $c_s^{(2)} = 3464$, $\rho^{(1)} = 2600$, and $\rho^{(2)} = 2700$.

The solution is driven by a point moment tensor source,

$$
\mathbf{f}(\mathbf{x}, t) = g(t) \begin{pmatrix} 0 & m_{xy} & 0 \\ m_{xy} & 0 & 0 \\ 0 & 0 & 0 \end{pmatrix} \nabla \delta(\mathbf{x} - \mathbf{x}_s), \tag{4.5}
$$

located at $\mathbf{x}_s = (x_s, y_s, z_s) = (20, 20, 2) \cdot 10^3$, with amplitude $m_{xy} = 10^{18}$. The source time function is the Gaussian,

$$g(t) = \frac{1}{2\pi\sigma} e^{(t-t_0)^2/2\sigma^2}, \qquad \sigma = 0.12, \qquad t_0 = 0.72. \tag{4.6}$$

We estimate the dominant frequency in the Gaussian by $f_0 = 1/(2\pi\sigma) \approx 1.33$ and the highest significant frequency by $f_{\max} \approx 2.5 f_0 \approx 3.32$, which corresponds to a shortest shear wave length of $\min c_s / f_{\max} \approx 2000/3.32 \approx 603.2$.

We choose the computational domain to be $(x,y,z) \in [0,4\cdot10^4] \times [0,4\cdot10^4] \times [0,1.5\cdot10^4]$. Super-grid layers of width $5\cdot10^3$ are used on all sides, except at $z = 0$, where we impose a free surface boundary condition. As a result, the domain of interest becomes $5\cdot10^3 \leq (x,y) \leq 3.5\cdot10^4$, and $0 \leq z \leq 10^4$. The simulations are run to time $t = 20$.

In Fig. 6 we show snapshots of the magnitude of the numerical solution with grid size $h = 50$ and sixth order dissipation with $\gamma_6 = 5\cdot10^{-3}$. The solution is shown along the free surface ($z = 0$) and in the vertical plane $y = 2\cdot10^4$. Due to the vertical variation of the material velocity, the solution has much more structure than the solution of Lamb's problem. The source is centered in the fast layer between $z_1 = 1000$ and $z_2 = 3000$ and generates head waves that are transmitted into the slower layers above and below. As the waves propagate further downwards, they speed up again as they enter the fast material for $z > 5000$. Several sets of surface and interface waves can be identified in the solution. We remark that no reflected waves are visible in the domain of interest after time $t \approx 15.5$.

No analytical solution is available for this problem. Instead we assess the convergence rate by comparing solutions on grids of three different grid sizes: $h = 100$, $h = 50$, and $h = 25$. According to the above estimate of the shortest shear wave length, these grid sizes correspond to approximately 6, 12, and 24 grid points per wave length.

We assume that the numerical solution, u_h, is a pth order accurate approximation of the solution of the continuous problem, u, and that the relation

$$u_h \approx u + h^p r, \tag{4.7}$$

holds, where r is a function that can be bounded independently of the grid size, h. It follows from (4.7) that $u_{2h} \approx u + 2^p h^p r$ and $u_{4h} \approx u + 4^p h^p r$. Therefore,

$$\frac{\|u_{4h} - u_h\|}{\|u_{2h} - u_h\|} \approx \frac{4^p - 1}{2^p - 1} = 2^p + 1,$$

and we can estimate the convergence rate by $p \approx \log_2(\|u_{4h} - u_h\| / \|u_{2h} - u_h\| - 1)$.

Because it is impractical to store the numerical solution at all points in space and time, we will limit our investigation to study the convergence of the time-dependent solution at fixed locations along the intersection between the free surface, $z = 0$, and the boundary of the domain of interest, $x = 3.5\cdot10^4$. For each grid size, we record the solution at seven equally spaced locations between $y_1 = 5\cdot10^3$ and the symmetry line $y_7 = 2\cdot10^4$,

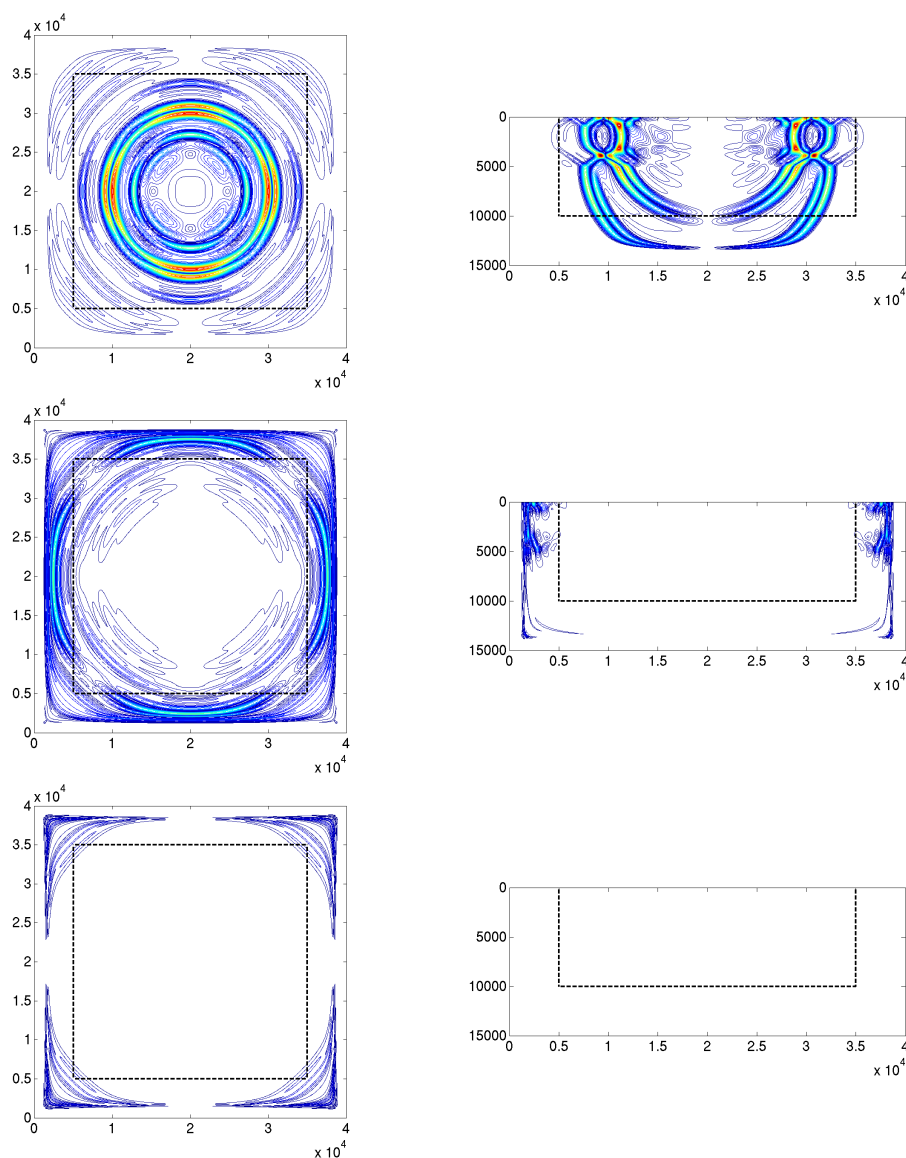$$y_k = 5\cdot10^3 + (k-1)2.5\cdot10^3, \qquad k = 1,2,\cdots,7.$$

Figure 6: Magnitude of the displacement in the layered material at times 5.035, 10.07, and 15.105 (top to bottom) in the $z=0$ plane (left) and the $y=2\cdot10^4$ plane (right). The dashed lines indicate the boundaries of the super-grid layers, which have thickness $\ell=5\cdot10^3$. The contour levels are the same in all plots and are spaced between 0.05 (dark blue) and 1.85 (red) with step size 0.05.

For example, Fig. 7 shows the Cartesian components of the solution as function of time, at the location $(x_4,y_4,z_4)=(3.5,1.25,0)\cdot10^4$.

On the right side of Fig. 7 we show the difference between the solutions computed with grid sizes $h=50$ and $h=25$. Note that the difference is significantly smaller than the solution itself, indicating that it is well-resolved on the grid.
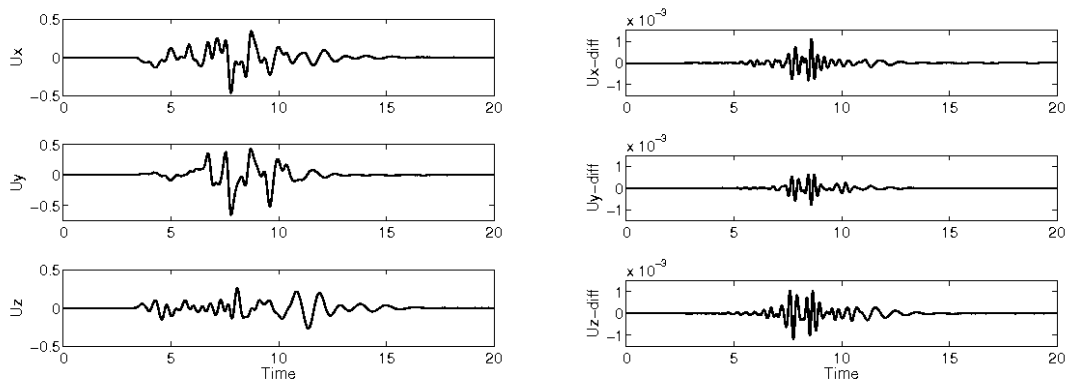
Figure 7: Solution at $(x_4, y_4, z_4) = (3.5, 1.25, 0) \cdot 10^4$ as function of time, computed with grid size $h = 50$ (left). Difference between the numerical solutions computed with grid size $h = 50$ and $h = 25$ (right).

Table 2: The L_2-norm of the difference between the numerical solutions at the locations (x_k, y_k, z_k), where $x_k = 3.5 \cdot 10^4$ and $z_k = 0$. Here, $p = \log_2(\text{ratio} - 1)$.

Location	y_k	$\|u_{4h} - u_h\|_2$	$\|u_{2h} - u_h\|_2$	ratio	p
1	$0.5 \cdot 10^4$	$4.567 \cdot 10^{-3}$	$2.640 \cdot 10^{-4}$	17.302	4.03
2	$0.75 \cdot 10^4$	$3.767 \cdot 10^{-3}$	$2.188 \cdot 10^{-4}$	17.213	4.02
3	$1 \cdot 10^4$	$3.903 \cdot 10^{-3}$	$2.269 \cdot 10^{-4}$	17.197	4.01
4	$1.25 \cdot 10^4$	$4.284 \cdot 10^{-3}$	$2.538 \cdot 10^{-4}$	16.882	3.99
5	$1.5 \cdot 10^4$	$3.267 \cdot 10^{-3}$	$2.096 \cdot 10^{-4}$	15.580	3.87
6	$1.75 \cdot 10^4$	$2.643 \cdot 10^{-3}$	$2.212 \cdot 10^{-4}$	11.950	3.45
7	$2 \cdot 10^4$	$2.679 \cdot 10^{-3}$	$2.456 \cdot 10^{-4}$	10.906	3.31

In Table 2 we report the L_2 norm of the differences between the numerical solutions at the seven locations. It is interesting to notice that the numerical solutions seem to converge better near the corner of the domain of interest. For locations y_1-y_4 we observe close to perfect fourth order rate of convergence. The rate for y_5-y_7 is slightly lower and goes down to about 3.3 on the symmetry line $y_7 = 2 \cdot 10^4$.

Estimating the convergence rate without access to an analytical solution requires the solution to be sufficiently well resolved on all grids. From the snapshots in Fig. 6 we observe that the surface waves are stronger along the symmetry lines than along the diagonal. Since they have slightly shorter wave lengths than the shear waves, it is possible that the surface waves are only marginally resolved on the coarsest grid. This may explain the slightly slower convergence rates near $y = 2 \cdot 10^4$. Nevertheless, we conclude that the super-grid approach is robust and leads to very small artificial reflections, also when the material model is heterogeneous.

5   Conclusions

We have developed a new a finite difference method to approximate the elastic wave equation with super-grid layers. The method combines fourth order accurate summation by parts (SBP) operators [17] with centered fourth order accurate finite difference formulas in the interior of the domain. To make the implementation of the method more efficient and greatly simplified in multi-dimensional domains, our main idea is to only use SBP operators near the physical free surface boundary. The centered finite difference formulas are used all the way up to the artificial super-grid boundaries, where the computational domain is truncated. This approach is made possible by enforcing homogeneous Dirichlet boundary conditions at several grid points outside the super-grid boundaries. Even though the overall discretization does not satisfy the principle of SBP, we have proven by energy estimates that the fully discrete approximation is stable.

One very desirable property of the super-grid method is that, with a wide enough layer, the modeling error from truncating the domain can be made as small as, or smaller than, the wave propagation errors from the interior scheme. This allows the total error in the solution to converge with full order of accuracy as the grid size tends to zero. As shown in the numerical experiments, fourth order accuracy can be achieved with a sixth order artificial damping term, if the super-grid layer has a constant thickness, i.e., independent of the grid size. This thickness can be considerably thinner than the trivial layer, which would be as wide as the distance traveled by the fastest wave over the duration of the entire simulation. However, while the modeling error is reduced by making the super-grid layer thicker, it also increases the computational cost and storage requirements of the simulation. There is therefore a trade-off between computational cost and accuracy of the solution, which is tunable by only changing one parameter, i.e., the width of the super-grid layers.

The super-grid approach can be generalized to curvilinear coordinates. This allows the free surface condition to be imposed on a non-planar surface, which for example is very desirable for modeling seismic wave propagation in the presence of realistic topography. The curvilinear super-grid approach has been implemented as part of the open source code SW4 [15].

The basic finite difference method itself could be generalized from fourth to higher order accuracy. All the summation by parts operators, and the modified equation based time stepping method, are available to at least sixth order of accuracy. The order of the dissipation operator in the super-grid layer would also need to be increased to match a higher order accurate interior scheme. This can be done in a straight forward way by noting that the $2p$ order dissipation operator gives a $2p-1$ order truncation error in the super-grid layers. Since these errors can propagate into the domain of interest, it is necessary to choose p such that $2p-1$ is larger than or equal to the expected convergence rate of the interior difference scheme. For example, to obtain overall sixth order of accuracy, it would be necessary to use an eight order artificial dissipation operator.

Additional extensions of the current work could include a more detailed analysis of

the modeling error from truncating the domain. In particular it would be desirable to establish a mathematical proof of our numerical observation that the solution converges with optimal rate, if the super-grid layer is sufficiently wide.

A Proofs of lemmas and theorems

A.1 Properties of $G(\mu)u$

We simplify the notation by first analyzing the function $K_1(v,u):=(v,G(\mu)u)_{h1}$. The finite difference operator $G(\mu)u_j$, defined by (2.9), can be written as a sum of three difference operators

$$G(\mu)u_j = D^{(x1)}\left(\mu_j D^{(x1)}u_j\right) + \frac{h^4}{18}D_+D_-D_+\left(\tilde{\mu}_j D_-D_+D_-u_j\right)$$
$$- \frac{h^6}{144}(D_+D_-)^2\left(\mu_j(D_+D_-)^2 u_j\right), \tag{A.1}$$

where $\tilde{\mu}_j = (\mu_j + \mu_{j-1})/2$. Here, D_+ and D_- denote the standard forward and backward divided difference operators. The term $D^{(x1)}w_j$ is a centered fourth order accurate approximation of $w_\xi(\xi_j)$. It can be written

$$D^{(x1)}w_j := D_0 w_j - \frac{h^2}{6}D_0 D_+D_- w_j, \qquad D_0 = \frac{1}{2}(D_+ + D_-). \tag{A.2}$$

In the following we set $N = N_x$.

We want to analyze $G(\mu)u_j$ for $j = 1,2,\cdots,N$. We first comment on the width of the stencil. The terms $D^{(x1)}\mu_j D^{(x1)}u_j$ and $(D+D)^2\mu_j(D+D-)^2u_j$ are both nine points wide. But the sum of the two is only seven point wide, since the outermost points in the stencils have weights of equal magnitude but opposite signs. Similarly, the sum of these two nine-point stencils and the seven point stencil, $D_+D_-D_+(\tilde{\mu}_j D_-D_+D_-u_j)$, has zero weights on the outermost terms, making the resulting stencil five points wide.

Since $G(\mu)u_j$ is a five point formula, its values at the interior points $1 \leq j \leq N$ are only influenced by u_q for $-1 \leq q \leq N+2$. We next treat the operators term by term. For simplicity, we introduce some additional artificial ghost points. Note that this is not strictly necessary, because $G(\mu)u_j$ is a five point formula, but it simplifies the presentation. The boundary condition $B_{sg}(u) = \mathbf{0}$ sets $u_{-1} = u_0 = 0$ and $u_{N+1} = u_{N+2} = 0$. However, we can impose boundary conditions at additional ghost points without changing $G(\mu)u_j$ for $j = 1,2,\cdots,N$. In particular, we choose to replace $B_{sg}(u) = \mathbf{0}$ and $B_{sg}(v) = \mathbf{0}$ by imposing homogeneous Dirichlet conditions at four ghost points

$$u_{-3} = u_{-2} = u_{-1} = u_0 = 0, \qquad v_{-3} = v_{-2} = v_{-1} = v_0 = 0, \tag{A.3}$$
$$u_{N+1} = u_{N+2} = u_{N+3} = u_{N+4} = 0, \qquad v_{N+1} = v_{N+2} = v_{N+3} = v_{N+4} = 0. \tag{A.4}$$

It is convenient to analyze $G(\mu)u_j$ by studying each term on the right hand side of (A.1) independently. We focus on the properties of $G(\mu)u_j$ near the left boundary, and we extend the grid functions to the semi-infinite domain $j \geq -3$ subject to the boundary conditions (A.3). We modify the scalar product to be

$$(u,v)_{h0} = h \sum_{j=1}^{\infty} u_j v_j. \tag{A.5}$$

In this scalar product, the basic forward, backward and centered divided difference operators satisfy the SBP parts identities

$$(v,D_+w)_{h0} = -(D_-v,w)_{h0} - w_1 v_0,$$
$$(v,D_-w)_{h0} = -(D_+v,w)_{h0} - w_0 v_1,$$
$$(v,D_0w)_{h0} = -(D_0v,w)_{h0} - \frac{1}{2}(w_0 v_1 + w_1 v_0). \tag{A.6}$$

Repeated use of these identities and boundary condition (A.3) lead to the relations

$$\left(v,D^{(x1)}(\mu D^{(x1)}u)\right)_{h0} = -\left(D^{(x1)}v,\mu D^{(x1)}u\right)_{h0} - J_1, \tag{A.7}$$

$$(v,D_+D_-D_+(\tilde{\mu}D_-D_+D_-u))_{h0} = -(D_-D_+D_-v,\tilde{\mu}D_-D_+D_-u)_{h0} - J_2, \tag{A.8}$$

$$\left(v,(D_+D_-)^2\left(\mu(D_+D_-)^2u\right)\right)_{h0} = \left((D_+D_-)^2v,\mu(D_+D_-)^2u\right)_{h0} + J_3. \tag{A.9}$$

The boundary terms satisfy

$$J_1 = \frac{1}{144h}\left(\mu_0(u_2-8u_1)(v_2-8v_1) + \mu_{-1}u_1 v_1\right),$$
$$J_2 = \frac{1}{h^5}\left(\mu_{-1/2}u_1 v_1\right),$$
$$J_3 = \frac{1}{h^7}\left(\mu_{-1}u_1 v_1 + \mu_0(u_2-4u_1)(v_2-4v_1)\right).$$

By collecting terms,

$$(v,G(\mu)u)_{h0} = -\left(D^{(x1)}v,\mu D^{(x1)}u\right)_{h0} - \frac{h^4}{18}(D_-D_+D_-v,\tilde{\mu}D_-D_+D_-u)_{h0}$$
$$- \frac{h^6}{144}\left((D_+D_-)^2v,\mu(D_+D_-)^2u\right)_{h0} - J, \tag{A.10}$$

where the boundary term satisfies $J = J_1 + h^4 J_2/18 + h^6 J_3/144$. All terms in (A.10) are symmetric in u and v. Since $\mu > 0$, all terms are negative or zero if $u = v$. The contributions from the right boundary can be analyzed in the same way. Collecting all contributions to $(v,G(\mu)u)_{h1}$ shows that the function K_1 is symmetric, i.e.,

$$K_1(v,u) := -(v,G(\mu)u)_{h1}, \qquad K_1(v,u) = K_1(u,v).$$

¿From the above construction, it is clear that $K_1(u,u) \geq 0$. It remains to show that $K_1(u,u)$ is positive definite, i.e., $K_1(u,u) = 0$ if and only if $u = 0$. Obviously, $K_1(u,u) = 0$ if $u = 0$. Because $K_1(u,u)$ is a sum of non-negative terms, it can only be zero if each term is zero. We choose to study the term

$$T_1(u) := (D_-D_+D_-u, \tilde{\mu}D_-D_+D_-u)_{h1} = h\sum_{j=1}^{N} \mu_{j-1/2}\left(D_-D_+D_-u_j\right)^2.$$

The difference equation $D_-D_+D_-u_j = 0$ has the general solution $u_j = \alpha + j\beta + j^2\gamma$ where α, β, and γ are constants. Because $T_1(u)$ only depends on the ghost point values u_{-1}, u_0, and u_{N+1}, the boundary condition $B_{sg}(u) = \mathbf{0}$ gives the linear system

$$\alpha - \beta + \gamma = 0, \tag{A.11}$$

$$\alpha = 0, \tag{A.12}$$

$$\alpha + (N+1)\beta + (N+1)^2\gamma = 0. \tag{A.13}$$

It is straight forward to see that this system only has the trivial solution $\alpha = \beta = \gamma = 0$. We conclude that $T_1(u) = 0$ if and only if $u = 0$. Hence, $K_1(u,u) = 0$ if and only if $u = 0$.

Since $\phi_j = \phi(\xi_j) \geq \varepsilon_L > 0$, the same arguments apply to the function $K_0(v,u) = (v, G(\phi\mu)u)_{h1}$. This proves the lemma.

A.2 The artificial dissipation operator Q_{2p}

We apply the same technique as in Section A.1 and start by studying the boundary terms due to the left boundary, using the scalar product (A.5). For a fourth order dissipation, $p = 2$, and we define $w_j = \sigma_j\rho_j D_+D_-u_j$. We have,

$$(v, Q_4 u)_{h0} = (v, D_+D_- w)_{h0}.$$

Combining the first two summation by parts rules in (A.6) gives

$$(v, D_+D_- w)_{h0} = (D_+D_- v, w)_{h0} - v_0 D_- w_1 + w_0 D_- v_1.$$

Because v satisfies the boundary condition $B_{sg}(v) = \mathbf{0}$, we have $v_0 = 0$. Therefore, the first boundary term is zero. For the second boundary term we have $D_- v_1 = v_1/h$. It can be further simplified because $B_{sg}(u) = \mathbf{0}$, so $u_{-1} = u_0 = 0$. Therefore, $w_0 = \sigma_0\rho_0 u_1/h^2$ and we obtain

$$(v, Q_4 u))_{h0} = (v, D_+D_- w)_{h0} = (D_+D_- v, \sigma\rho D_+D_- u)_{h0} + v_1 u_1 \frac{\sigma_0\rho_0}{h^3}.$$

All terms on the right hand side are symmetric in u and v. Furthermore, they are non-negative when $u = v$. Hence, there is a function $C_0(u,v)$ that does not depend on the ghost point values of u or v, such that

$$(v, Q_4 u))_{h0} = C_0(v,u), \qquad C_0(u,v) = C_0(v,u), \qquad C_0(u,u) \geq 0.$$

The influence of the right boundary can be analyzed in the same way. The same approach applies to all dissipation operators of order $2p$, $p \geq 1$. This proves the lemma.

A.3   One-dimensional energy estimate

Assuming $F(t)=0$, we derive an energy estimate for (2.23) by forming the scalar product between $(\bar{u}^{n+1}-\bar{u}^{n-1})\Phi^{-1}$ and (2.23) (note that Φ is non-singular because $\phi_j \geq \varepsilon_L > 0$). For the left hand side, we get

$$\frac{1}{\Delta_t^2}\left(\bar{u}^{n+1}-\bar{u}^{n-1},\Phi^{-1}M(\bar{u}^{n+1}-2\bar{u}^n+\bar{u}^{n-1})\right)_{h1}$$

$$=\frac{1}{\Delta_t^2}\left(\bar{u}^{n+1}-\bar{u}^n,\Phi^{-1}M(\bar{u}^{n+1}-\bar{u}^n)\right)_{h1}-\frac{1}{\Delta_t^2}\left(\bar{u}^n-\bar{u}^{n-1},\Phi^{-1}M(\bar{u}^n-\bar{u}^{n-1})\right)_{h1}. \quad (A.14)$$

Because the matrices K, Φ, and M are symmetric, the first two terms on the right hand side of (2.23) become

$$\left(\bar{u}^{n+1}-\bar{u}^{n-1},-K\bar{u}^n+\frac{\Delta_t^2}{12}KM^{-1}\Phi K\bar{u}^n\right)_{h1}$$

$$=\left(\bar{u}^{n+1},-K\bar{u}^n+\frac{\Delta_t^2}{12}KM^{-1}\Phi K\bar{u}^n\right)_{h1}-\left(\bar{u}^n,-K\bar{u}^{n-1}+\frac{\Delta_t^2}{12}KM^{-1}\Phi K\bar{u}^{n-1}\right)_{h1}, \quad (A.15)$$

where we have used $\Phi M^{-1}=M^{-1}\Phi$.

To analyze the dissipative term (last term on the right hand side of (2.23)), it is helpful to first consider an expression of the type $(\bar{x}+\bar{y},C\bar{y})_{h1}$, where $C=C_{2p}$. We have

$$(\bar{x}+\bar{y},C\bar{y})_{h1}=(\bar{x}+\bar{y},C(\bar{x}+\bar{y}))_{h1}-(\bar{x}+\bar{y},C\bar{x})_{h1}.$$

Also, $(\bar{x}+\bar{y},C\bar{y})_{h1}=(\bar{x},C\bar{y})_{h1}+(\bar{y},C\bar{y})_{h1}$. Because C is symmetric,

$$(\bar{x}+\bar{y},C\bar{y})_{h1}=\frac{1}{2}(\bar{x}+\bar{y},C(\bar{x}+\bar{y}))_{h1}-\frac{1}{2}(\bar{x}+\bar{y},C\bar{x})_{h1}+\frac{1}{2}(\bar{x},C\bar{y})_{h1}+\frac{1}{2}(\bar{y},C\bar{y})_{h1}$$

$$=\frac{1}{2}(\bar{x}+\bar{y},C(\bar{x}+\bar{y}))_{h1}-\frac{1}{2}(\bar{x},C\bar{x})_{h1}+\frac{1}{2}(\bar{y},C\bar{y})_{h1}.$$

Now take $\bar{x}=\bar{u}^{n+1}-\bar{u}^n$ and $\bar{y}=\bar{u}^n-\bar{u}^{n-1}$. The expression for the dissipative term in (2.22) becomes

$$\left(\bar{u}^{n+1}-\bar{u}^{n-1},C_{2p}\left(\bar{u}^n-\bar{u}^{n-1}\right)\right)_{h1}$$

$$=\frac{1}{2}\left(\bar{u}^{n+1}-\bar{u}^{n-1},C_{2p}\left(\bar{u}^{n+1}-\bar{u}^{n-1}\right)\right)_{h1}-\frac{1}{2}\left(\bar{u}^{n+1}-\bar{u}^n,C_{2p}\left(\bar{u}^{n+1}-\bar{u}^n\right)\right)_{h1}$$

$$+\frac{1}{2}\left(\bar{u}^n-\bar{u}^{n-1},C_{2p}\left(\bar{u}^n-\bar{u}^{n-1}\right)\right)_{h1}. \quad (A.16)$$

By inspection of the three terms (A.14), (A.15), and (A.16), it is natural to define the discrete energy according to (2.25). After re-arranging the terms of (A.14), (A.15), and (A.16), we arrive at the energy estimate (2.29).

To analyze the properties of $e^{n+1/2}$, we re-write the terms of (2.25) that involve K. Because K is symmetric,

$$(\bar{u}^{n+1}, K\bar{u}^n)_{h1} = \frac{1}{4}(\bar{u}^{n+1} + \bar{u}^n, K(\bar{u}^{n+1} + \bar{u}^n))_{h1} - \frac{1}{4}(\bar{u}^{n+1} - \bar{u}^n, K(\bar{u}^{n+1} - \bar{u}^n))_{h1}.$$

The same procedure applies to the terms involving the matrix $KM^{-1}\Phi K$, which also is symmetric because $\Phi M^{-1} = M^{-1}\Phi$. The discrete energy $e^{n+1/2}$ can therefore be grouped into two terms

$$e^{n+1/2} = \left(\bar{u}^{n+1} - \bar{u}^n, \left(\frac{1}{\Delta_t^2}\Phi^{-1}M - \frac{1}{4}K + \frac{\Delta_t^2}{48}KM^{-1}\Phi K - \frac{\varepsilon}{2\Delta_t}C_{2p}\right)(\bar{u}^{n+1} - \bar{u}^n)\right)_{h1}$$
$$+ \left(\bar{u}^{n+1} + \bar{u}^n, \left(\frac{1}{4}K - \frac{\Delta_t^2}{48}KM^{-1}\Phi K\right)(\bar{u}^{n+1} + \bar{u}^n)\right)_{h1}.$$

We have $e^{n+1/2} > 0$ if both terms are positive. By taking $\bar{w} = \bar{u}^{n+1} - \bar{u}^n$, we see that the first term is positive if (2.26) is satisfied. Setting $\bar{w} = \bar{u}^{n+1} + \bar{u}^n$ shows that the second term is positive if (2.27) is satisfied. This completes the proof.

A.4 Anti-symmetry of $D^{(x)}$

We first prove the corresponding lemma for the 1-D operator (A.2), where u and v are 1-D grid functions satisfying the boundary conditions $B_{sg}(u) = 0$ and $B_{sg}(v) = 0$. By expanding the terms in the scalar product and rearranging them,

$$\left(v, D^{(x1)}u\right)_{h1}$$
$$= \frac{1}{12}\sum_{i=1}^{N} v_i(u_{i-2} - 8u_{i-1} + 8u_{i+1} - u_{i+2})$$
$$= \frac{1}{12}[u_{-1}v_1 + u_1v_{-1} + u_0(-8v_1 + v_2) + v_0(-8u_1 + u_2)] + \frac{1}{12}\sum_{i=1}^{N} u_i(-v_{i-2} + 8v_{i-1} - 8v_{i+1} + v_{i+2})$$
$$+ \frac{1}{12}[-u_{N+2}v_N - v_{N+2}u_N + u_{N+1}(8v_N - v_{N-1}) + v_{N+1}(8u_N - u_{N-1})]. \tag{A.17}$$

The boundary terms are equal to zero because $B_{sg}(u) = 0$ and $B_{sg}(v) = 0$ imply $u_{-1} = u_0 = v_{-1} = v_0 = 0$ and $u_{N+2} = u_{N+1} = v_{N+2} = v_{N+1} = 0$. Hence, we obtain

$$\left(v, D^{(x1)}u\right)_{h1} = -\left(D^{(x1)}v, u\right)_{h1}.$$

Trivial generalizations extend the proof to two-dimensional grid functions.

A.5   Symmetry of the two-dimensional discretization

First, we need the following refinement of (3.23),

$$\left(v,G^{(y)}(\mu)u\right)_{hw} = -\left(D^{(y)}v,\mu D^{(y)}u\right)_{hw} - \left(v,P^{(y)}(\mu)u\right)_h - h\sum_{i=1}^{N_x}\mu_{i,1}v_{i,1}B^{(y)}u_{i,1}, \quad (A.18)$$

which was proven in [17]. Here $P^{(y)}(\mu)$ is an operator acting in the y-direction, which is positive definite in the un-weighted scalar product $(u,v)_h$,

$$(u,v)_h = h^2\sum_{i=1}^{N_x}\sum_{j=1}^{N_y}u_{i,j}v_{i,j}.$$

For details, see [17]. The identity corresponding to (A.18) for the operator in the x-direction does not have a boundary term. The proof is a trivial generalization of the result in Appendix A.1.

To prove (3.26), we introduce the grid functions $\mathbf{u} = (u^{(x)}, u^{(y)})^T$, $\mathbf{w} = (w^{(x)}, w^{(y)})^T$, and write out the components of (3.26) as

$$\left(\mathbf{w},\frac{1}{\phi^{(x)}\phi^{(y)}}\mathbf{L}_h\mathbf{u}\right)_{hw} = \left(w^{(x)},\frac{1}{\phi^{(x)}\phi^{(y)}}L_h^{(u)}\mathbf{u}\right)_{hw} + \left(w^{(y)},\frac{1}{\phi^{(x)}\phi^{(y)}}L_h^{(v)}\mathbf{u}\right)_{hw}. \quad (A.19)$$

The first term on the right hand side is expanded as

$$\left(w^{(x)},\frac{1}{\phi^{(x)}\phi^{(y)}}L_h^{(u)}\mathbf{u}\right)_{hw}$$
$$= \left(w^{(x)},\frac{1}{\phi^{(y)}}G^{(x)}\left(\phi^{(x)}(2\mu+\lambda)\right)u^{(x)}\right)_{hw} + \left(w^{(x)},D^{(x)}\lambda D^{(y)}u^{(y)}\right)_{hw}$$
$$+ \left(w^{(x)},D^{(y)}\mu D^{(x)}u^{(y)}\right)_{hw} + \left(w^{(x)},\frac{1}{\phi^{(x)}}G^{(y)}\left(\phi^{(y)}\mu\right)u^{(x)}\right)_{hw}, \quad (A.20)$$

where we have used that $\phi^{(x)}$ does not depend on η_j, and $\phi^{(y)}$ does not depend on ξ_i. Next the summation by parts identities are used on each term in (A.20). As shown in Lemmas 2.1, 2.2, and 3.2, there are no boundary terms from operators in the x-direction. The y-direction formulas are given in equations (3.24), (3.25), and (A.18). The resulting

expression is

$$
\left(w^{(x)}, \frac{1}{\phi^{(x)}\phi^{(y)}} L_h^{(u)} \mathbf{u} \right)_{hw}
$$

$$
= -\left(D^{(x)}w^{(x)}, \frac{\phi^{(x)}}{\phi^{(y)}}(2\mu+\lambda)D^{(x)}u^{(x)} \right)_{hw} - \left(w^{(x)}, \frac{1}{\phi^{(y)}}P^{(x)}(\phi^{(x)}(2\mu+\lambda))u^{(x)} \right)_{h}
$$

$$
-\left(D^{(x)}w^{(x)}, \lambda D^{(y)}u^{(y)} \right)_{hw} - \left(D^{(y)}w^{(x)}, \mu D^{(x)}u^{(y)} \right)_{hw} - \left(D^{(y)}w^{(x)}, \frac{\phi^{(y)}}{\phi^{(x)}}\mu D^{(y)}u^{(x)} \right)_{hw}
$$

$$
-\left(w^{(x)}, \frac{1}{\phi^{(x)}}P^{(y)}(\phi^{(y)}\mu)u^{(x)} \right)_{h} - h\sum_{i=1}^{N_x} w_{i,1}^{(x)} \frac{\mu_{i,1}}{\phi_i^{(x)}} \left(\phi_i^{(x)}D^{(x)}u_{i,1}^{(y)} + \phi_1^{(y)}B^{(y)}u_{i,1}^{(x)} \right). \quad \text{(A.21)}
$$

By performing a similar expansion of the second term on the right hand side of (A.19), adding together the results, and completing the squares, we arrive at the final expression

$$
\left(\mathbf{w}, \frac{1}{\phi^{(x)}\phi^{(y)}}\mathbf{L}_h\mathbf{u} \right)_{hw} = E_h + P_h + T_h,
$$

where

$$
E_h = -\left(\phi^{(x)}D^{(x)}w^{(x)} + \phi^{(y)}D^{(y)}w^{(y)}, \frac{\lambda}{\phi^{(x)}\phi^{(y)}}[\phi^{(x)}D^{(x)}u^{(x)} + \phi^{(y)}D^{(y)}u^{(y)}] \right)_{hw}
$$

$$
-\left(\phi^{(y)}D^{(y)}w^{(x)} + \phi^{(x)}D^{(x)}w^{(y)}, \frac{\mu}{\phi^{(x)}\phi^{(y)}}[\phi^{(y)}D^{(y)}u^{(x)} + \phi^{(x)}D^{(x)}u^{(y)}] \right)_{hw}
$$

$$
-\left(\phi^{(x)}D^{(x)}w^{(x)}, \frac{2\mu}{\phi^{(x)}\phi^{(y)}}[\phi^{(x)}D^{(x)}u^{(x)}] \right)_{hw}
$$

$$
-\left(\phi^{(y)}D^{(y)}w^{(y)}, \frac{2\mu}{\phi^{(x)}\phi^{(y)}}[\phi^{(y)}D^{(y)}u^{(y)}] \right)_{hw}, \quad \text{(A.22)}
$$

and

$$
P_h = -\left(w^{(x)}, \frac{1}{\phi^{(y)}}P^{(x)}(\phi^{(x)}(2\mu+\lambda))u^{(x)} \right)_{h} - \left(w^{(x)}, \frac{1}{\phi^{(x)}}P^{(y)}(\phi^{(y)}\mu)u^{(x)} \right)_{h}
$$

$$
-\left(w^{(y)}, \frac{1}{\phi^{(y)}}P^{(x)}(\phi^{(x)}\mu)u^{(y)} \right)_{h} - \left(w^{(y)}, \frac{1}{\phi^{(x)}}P^{(y)}(\phi^{(y)}(2\mu+\lambda))u^{(y)} \right)_{h}. \quad \text{(A.23)}
$$

The boundary terms are

$$
T_h = -h\sum_{i=1}^{N_x} w_{i,1}^{(y)} \frac{1}{\phi_i^{(x)}} \left(\phi_i^{(x)}\lambda_{i,1}D^{(x)}u_{i,1}^{(x)} + \phi_1^{(y)}(2\mu_{i,1}+\lambda_{i,1})B^{(y)}u_{i,1}^{(y)} \right)
$$

$$
-h\sum_{i=1}^{N_x} w_{i,1}^{(x)} \frac{\mu_{i,1}}{\phi_i^{(x)}} \left(\phi_i^{(x)}D^{(x)}u_{i,1}^{(y)} + \phi_1^{(y)}B^{(y)}u_{i,1}^{(x)} \right), \quad \text{(A.24)}
$$

which vanish under the homogeneous boundary condition (3.15)–(3.16), because $\phi_1^{(y)} = 1$. Hence, we have

$$S_h(\mathbf{w}, \mathbf{u}) = -E_h - P_h.$$

Here E_h is an approximation of the spatial terms in the elastic energy (3.8), and P_h is symmetric in its arguments and positive definite.

The dissipation operator can similarly be expanded into the four terms

$$
\begin{aligned}
&\left(\mathbf{w}, \frac{1}{\phi^{(x)}\phi^{(y)}} \mathbf{Q}_{2p}(\mathbf{u}) \right)_{hw} \\
&= \left(w^{(x)}, \frac{1}{\phi^{(y)}} Q_{2p}^{(x)}(\sigma^{(x)}\rho)u^{(x)} \right)_{hw} + \left(w^{(x)}, \frac{1}{\phi^{(x)}} Q_{2p}^{(y)}(\sigma^{(y)}\rho)u^{(x)} \right)_{hw} \\
&\quad + \left(w^{(y)}, \frac{1}{\phi^{(y)}} Q_{2p}^{(x)}(\sigma^{(x)}\rho)u^{(y)} \right)_{hw} + \left(w^{(y)}, \frac{1}{\phi^{(x)}} Q_{2p}^{(y)}(\sigma^{(y)}\rho)u^{(y)} \right)_{hw}.
\end{aligned}
\tag{A.25}
$$

By applying Lemma 2.2 to each term, we see that the expression is symmetric and positive semi-definite. Note that although Lemma 2.2 holds in the unweighed norm, and (A.25) uses the weighted norm, there is no difficulty because the y-direction operators in (A.25) are zero near the boundary $\eta = 0$, where the norm is weighted.

Acknowledgments

References

[1] D. Appelö and T. Colonius. A high order super-grid-scale absorbing layer and its application to linear hyperbolic systems. J. Comput. Phys., 228:4200–4217, 2009.

[2] E. Bécache, S. Fauqueux, and P. Joly. Stability of perfectly matched layers, group velocities and anisotropic waves. J. Compt. Phys., 188:399–433, 2003.

[3] J. P. Berenger. A perfectly matched layer for the absorption of electromagnetic waves. J. Comput. Phys., 114:185–200, 1994.

[4] R. Clayton and B. Engquist. Absorbing boundary conditions for acoustic and elastic wave equations. Bull. Seismo. Soc. Amer., 67, 1977.

[5] A. Cemal Eringen and Erdoğan S. Şuhubi. Elastodynamics, Volume II. Elsevier, 1975.

[6] R. L. Higdon. Radiation boundary conditions for elastic wave propagation. SIAM J. Numer. Anal., 27:831–870, 1990.

[7] H.-O. Kreiss and J. Lorenz. Initial-Boundary Value Problems and the Navier-Stokes Equations. Academic Press, 1989.

[8] Horace Lamb. On the propagation of tremors over the surface of an elastic solid. Phil. Trans. Roy. Soc. London, Ser. A, 203, 1904.

[9] K. Mattsson, F. Ham, and G. Iaccarino. Stable and accurate wave-propagation in discontinuous media. J. Comput. Phys., 227:8753–8767, 2008.

[10] K. Mattsson and J. Nordström. Summation by parts operators for finite difference approximations of second derivatives. J. Comput. Phys., 199:503–540, 2004.

[11] Harold M. Mooney. Some numerical solutions for Lamb's problem. Bull. Seismo. Soc. Amer., 64, 1974.

[12] Netlib. Repository of scientific computing software. `http://www.netlib.org`.

[13] N. A. Petersson and B. Sjögreen. An energy absorbing far-field boundary condition for the elastic wave equation. Comm. Comput. Phys., 6:483–508, 2009.

[14] N. A. Petersson and B. Sjögreen. Stable grid refinement and singular source discretization for seismic wave simulations. Comm. Comput. Phys., 8(5):1074–1110, November 2010.

[15] N. A. Petersson and B. Sjögreen. User's guide to SW4, version 1.0. Technical Report LLNL-SM-642292, Lawrence Livermore National Laboratory, 2013. (Source code available from `computation.llnl.gov/casc/serpentine`).

[16] B. Sjögreen and N. A. Petersson. Perfectly matched layers for Maxwell's equations in second order formulation. J. Comput. Phys., 209:19–46, 2005.

[17] B. Sjögreen and N. A. Petersson. A fourth order accurate finite difference scheme for the elastic wave equation in second order formulation. J. Sci. Comput., 52:17–48, 2012. DOI 10.1007/s10915-011-9531-1.

[18] E. A. Skelton, S. D. M. Adams, and R. V. Craster. Guided elastic waves and perfectly matched layers. Wave Motion, 44:573–592, 2007.